Class I Myosins Have Overlapping and Specialized Functions in Left-Right Asymmetric Development in *Drosophila*

Takashi Okumura,*,[1,2] Takeshi Sasamura,*,†,[1] Momoko Inatomi,† Shunya Hozumi,*,[3] Mitsutoshi Nakamura,*,† Ryo Hatori,* Kiichiro Taniguchi,*,[4] Naotaka Nakazawa,* Emiko Suzuki,‡ Reo Maeda,* Tomoko Yamakawa,*,† and Kenji Matsuno*,†,[5]

*Department of Biological Science and Technology, Tokyo University of Science, Tokyo 125-1500, Japan, †Department of Biological Sciences, Graduate School of Science, Osaka University, Osaka 560-0043, Japan, and ‡Gene Network Laboratory, Structural Biology Center, National Institute of Genetics, and Department of Genetics SOKENDAI, Shizuoka 411-8540, Japan

ABSTRACT The class I myosin genes are conserved in diverse organisms, and their gene products are involved in actin dynamics, endocytosis, and signal transduction. *Drosophila melanogaster* has three class I myosin genes, *Myosin 31DF* (*Myo31DF*), *Myosin 61F* (*Myo61F*), and *Myosin 95E* (*Myo95E*). Myo31DF, Myo61F, and Myo95E belong to the Myosin ID, Myosin IC, and Myosin IB families, respectively. Previous loss-of-function analyses of *Myo31DF* and *Myo61F* revealed important roles in left–right (LR) asymmetric development and enterocyte maintenance, respectively. However, it was difficult to elucidate their roles *in vivo*, because of potential redundant activities. Here we generated class I myosin double and triple mutants to address this issue. We found that the triple mutant was viable and fertile, indicating that all three class I myosins were dispensable for survival. A loss-of-function analysis revealed further that *Myo31DF* and *Myo61F*, but not *Myo95E*, had redundant functions in promoting the dextral LR asymmetric development of the male genitalia. *Myo61F* overexpression is known to antagonize the dextral activity of *Myo31DF* in various *Drosophila* organs. Thus, the LR-reversing activity of overexpressed *Myo61F* may not reflect its physiological function. The endogenous activity of Myo61F in promoting dextral LR asymmetric development was observed in the male genitalia, but not the embryonic gut, another LR asymmetric organ. Thus, Myo61F and Myo31DF, but not Myo95E, play tissue-specific, redundant roles in LR asymmetric development. Our studies also revealed differential colocalization of the class I myosins with filamentous (F)-actin in the brush border of intestinal enterocytes.

KEYWORDS myosin I; *Myosin 31DF*; *Myosin 61F*; *Myosin 95E*; left-right asymmetry

THE class I myosin genes encode myosin heavy chains, which are conserved in phylogenetically diverse organisms (Sellers 2000; Krendel and Mooseker 2005). The class I myosins are nonfilamentous, actin-based motor proteins and were the first discovered unconventional myosin proteins. These myosins are involved in a variety of cellular processes, such as cell migration, cell adhesion, and cell growth, through their regulation of actin dynamics, endocytosis, and signal transduction (Osherov and May 2000; Krendel and Mooseker 2005; Kim and Flavell 2008; McConnell and Tyska 2010).

The structure of the myosin I heavy chains is evolutionarily conserved and composed of head (or motor), neck, and tail domains (Figure 1A) (Coluccio 1997; Barylko *et al.* 2000). The head domain binds to filamentous (F)-actin and adenosine triphosphate (ATP), a common feature of myosin proteins (Figure 1A) (Mermall *et al.* 1998); the neck domain possesses one or more IQ motifs, which directly interact with calmodulin or calmodulin-related myosin light chains (Coluccio 1997; Barylko *et al.* 2000), and

doi: 10.1534/genetics.115.174698
Manuscript received March 31, 2014; accepted for publication February 4, 2015; published Early Online February 6, 2015.
Supporting information is available online at http://www.genetics.org/lookup/suppl/doi:10.1534/genetics.115.174698/-/DC1.
[1]These authors contributed equally to this work.
[2]Present address: Department of Chemistry and Biochemistry, Graduate School of Advanced Science and Engineering, Waseda University, 3-4-1 Okubo, Shinjuku-ku, Tokyo 169-8555, Japan.
[3]Present address: Department of Biological Science, Graduate School of Science, Hiroshima University, 1-3-1 Kagamiyama, Higashi-Hiroshima, Hiroshima 739-8511, Japan.
[4]Present address: Department of Life Science, Graduate School of Science, Gakushuin University, 1-5-1 Mejiro, Toshima-ku, Tokyo 171-8588, Japan.
[5]Corresponding author: Department of Biological Sciences, Graduate School of Science, Osaka University, 1-1 Machikaneyama-cho, Toyonaka, Osaka 560-0043, Japan. E-mail: kmatsuno@bio.sci.osaka-u.ac.jp

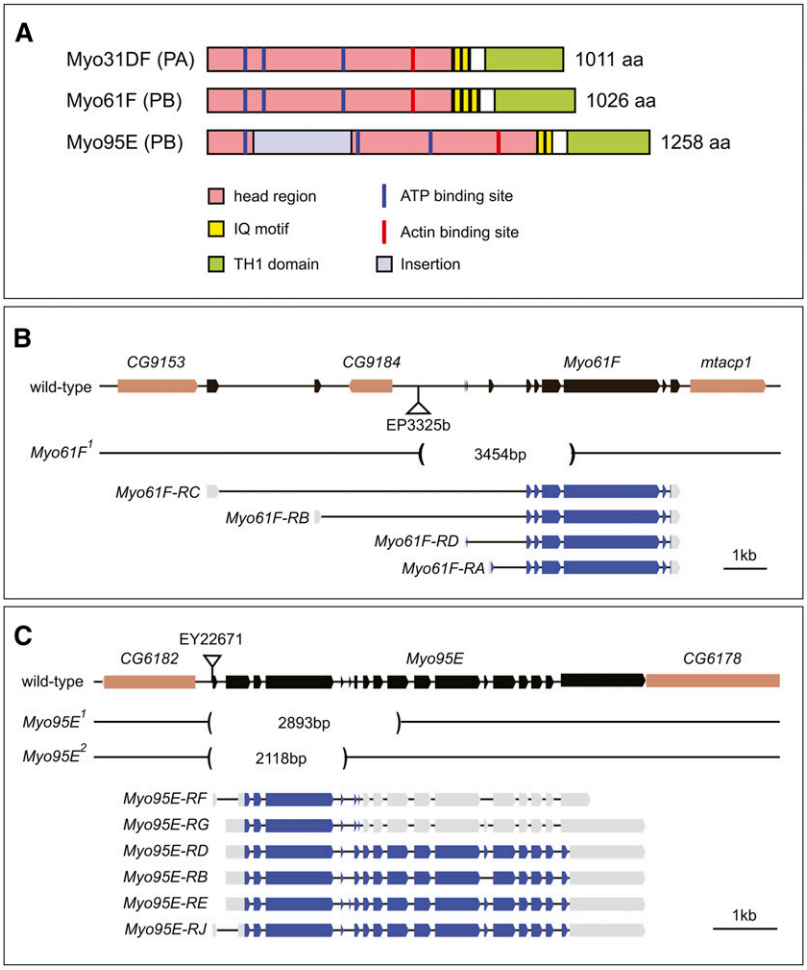

Figure 1 Deduced structures of the *Drosophila* myosin I family proteins and the genes and transcripts encoding them. (A) *Drosophila* Myo31DF-PA, Myo61F-PB, and Myo95E-PB structures, all of which possess characteristic domains/motifs/sites of class I myosins, including ATP- and actin-binding sites, IQ motifs, and TH1 domains, represented by the colors at the bottom. The insertion in Myo95E is shown in light purple. (B and C) Diagrams of the genomic regions of *Myo61F* (B) and *Myo95E* (C) loci. Exons of *Myo61F* and *Myo95E* are represented by black boxes. Neighboring genes are shown by light brown boxes. Deleted regions of $Myo61F^{1}$, $Myo95E^{1}$, and $Myo95E^{2}$, generated by the imprecise excision of EP3325b or EY22671, are indicated by parentheses, in which the length (in base pairs) of the deletion is indicated. Coding and noncoding regions in the four and six predicted transcripts of *Myo61F* and *Myo95E* are represented by blue and gray boxes, respectively.

the tail domains are divided into short and long types. Short tails contain a single tail homology 1 (TH1) domain, which is rich in basic residues and thought to interact with plasma membranes (Coluccio 1997; Barylko *et al.* 2000); while long tails contain the TH1 domain; a tail homology 2 (TH2) domain, which is proline-rich and binds to F-actin in an ATP-independent manner; and a tail homology 3 (TH3), or Src homology 3 (SH3) domain, at the C terminus (Coluccio 1997; Barylko *et al.* 2000).

In single-celled eukaryotes that have multiple myosin I genes, redundant roles of these genes have been reported (Novak *et al.* 1995; Geli and Riezman 1996; Goodson *et al.* 1996; Jung *et al.* 1996). *Saccharomyces cerevisiae* encodes two class I myosins that function redundantly in growth and endocytosis (Geli and Riezman 1996; Goodson *et al.* 1996), and *Dictyostelium* encodes multiple class I myosins I with overlapping functions in macropinocytosis (Novak *et al.* 1995; Jung *et al.* 1996). Eight class I myosins are expressed in humans and mice (Berg *et al.* 2001). Myosin IA is thought to maintain brush border structure and membrane tension and to power the release of vesicles from the tips of microvilli (Tyska *et al.* 2005; McConnell *et al.* 2009; Nambiar *et al.* 2009), while Myosin IB regulates the actin-dependent post-Golgi trafficking of cargo (Almeida *et al.* 2011). Myosin IC is involved in vesicle transport both in the fertilized egg of *Xenopus* and in mammalian cells (Bose *et al.* 2002; Sokac *et al.* 2006; Fan *et al.* 2012) and regulates ion channels in the hair cells of the inner ear (Gillespie and Cyr 2004). Interestingly, an isoform of Myosin IC localizes to the nucleus and contributes to transcription (Pestic-Dragovich *et al.* 2000; Philimonenko *et al.* 2004), and Myosin IF is involved in neutrophil migration (Kim *et al.* 2006). In addition, mutations in *Myosin IA*, *Myosin IC*, and *Myosin IF* are associated with hereditary hearing loss (Chen *et al.* 2001; Donaudy *et al.* 2003; Zadro *et al.* 2009). In vertebrates, each class I myosin is expressed in various cell types and has distinct functions that depend on their cellular context (Gillespie 2004; Philimonenko *et al.* 2004; Sokac *et al.* 2006). Even so, these multiple class I myosins are predicted to have overlapping functions, as found in yeast and *Dictyostelium* (Tyska *et al.* 2005; Nambiar *et al.* 2009; Chen *et al.* 2012), complicating the understanding of their *in vivo* roles (Kim and Flavell 2008). Thus, the knockout and analysis of multiple class I myosin genes in vertebrates would represent a major challenge.

Three class I myosin genes, *Myo31DF*, *Myo61F*, and *Myo95E* have been identified in *Drosophila* (Figure 1A) (Tzolovsky *et al.* 2002). *Myo31DF* and *Myo61F* are closely

related to the mammalian *Myosin ID* and *Myosin IC*, respectively (Morgan *et al.* 1994; Berg *et al.* 2001). However, the head domain of Myo95E contains an atypical insertion (Figure 1A) (Tzolovsky *et al.* 2002) (FlyBase, http://flybase.org/reports/FBgn0039157.html). All of these class I myosins possess short tails with characteristic motifs/sites such as the actin- and ATP-binding sites and the IQ motifs (Figure 1A) (Tzolovsky *et al.* 2002). *Myo31DF* is involved in the development of left–right (LR) asymmetry (Hozumi *et al.* 2006; Speder *et al.* 2006), and its loss leads to the LR inversion of several organs, including the embryonic gut, male genital plate, spermiduct, and testes (Hozumi *et al.* 2006; Speder *et al.* 2006). Myo61F is required for maintenance of the enterocyte brush border structure, as determined genetically (Hegan *et al.* 2007), while its roles in LR asymmetric development are mostly based on overexpression and RNA interference experiments (Hozumi *et al.* 2006, 2008; Petzoldt *et al.* 2012). Myo61F overexpression antagonizes Myo31DF's function, leading to LR inversion of the embryonic gut and the male genitalia (Hozumi *et al.* 2008; Petzoldt *et al.* 2012), and a model was proposed suggesting that overexpressed Myo61F prevents the binding of Myo31DF to adherens junction components, leading to impaired LR rotation of the male genitalia (Petzoldt *et al.* 2012). In contrast, no studies of *Myo95E* have been reported.

The limited number of class I myosin genes in *Drosophila* is an advantage for elucidating their functions and interactions *in vivo*. Here, we studied the roles of the three *Drosophila* class I myosins, using novel mutant alleles of *Myo61F* and *Myo95E*, as well as the previously isolated null mutant allele of *Myo31DF*.

Materials and Methods

Fly stocks

Flies were cultured on standard medium at 25°. Canton-S was the wild-type strain. The stocks carrying *P{EP}Myo61F^{EP3325a}*, *P{EPgy2}Myo95E^{EY22671}*, *patched* (*ptc*)^{16}, *Df(3L)BSC250* (uncovering the *Myo61F* locus), *Df(3R)Exel6198* (uncovering the *Myo95E* locus), *daughterless* (*da*)-*GAL4*, *Actin5C* (*Act5C*)-*GAL4*, *H{PDelta2-3}HoP8*, or *P{Delta2-3}99B* (stock nos. 17114, 22577, 35500, 23150, 7677, 5460, 4414, 2080, and 1610, respectively) were obtained from the Bloomington Stock Center. *white* (*w*)^{1118}, *roughoid* (*ru*)^{1} *hairy* (*h*)^{1} *scarlet* (*st*)^{1} *rosy* (*ry*)^{506} *ebony* (*e*)^{1}, and *sepia* (*se*)^{1} *spineless* (*ss*)^{1} *kidney* (*k*)^{1} *e^{s} rough* (*ro*)^{1} (stock nos. 150534, 105729, and 105998) were obtained from the *Drosophila* Genetic Resource Center. The other stocks used in this study were described previously: *Myo31DF^{L152}* (Hozumi *et al.* 2006), *Myo31DF^{K2}* (Speder *et al.* 2006), *UAS-Myo31DF-GFP* (Speder *et al.* 2006), *UAS-Myo31DF-mEGFP* (Taniguchi *et al.* 2011), *UAS-Myo61F* (Hozumi *et al.* 2006), *byn-GAL4* (Iwaki and Lengyel 2002), *24B-GAL4* (*how^{24B}*) (Fyrberg *et al.* 1997), *Abdominal-B* (*AbdB*)-*GAL4* (Foronda *et al.* 2006), *hedgehog* (*hh*)-*GAL4* (Suzanne *et al.* 2010), and *patched* (*ptc*)-*GAL4* (Johnson *et al.* 1995). *Df(3R)Exel6198* was balanced using *TM3*, *P{w[+mC]=sChFP}3* (Bloomington Stock Center). For the germline transformation of *UAS-Myo95E-RF*, *y^{1} M{vas-int.Dm}ZH-2A w**; *M{3xP3-RFP.attP'}ZH-51C* (Bloomington stock no. 24482) (Bischof *et al.* 2007) was used.

Constructs and germline transformation

UAS-Myo95E-RB and *UAS-Myo95E-RD* produce slightly different alternative splicing products of the *Myo95E* locus, which are both long isoforms of Myo95E, and *UAS-Myo95E-RF* produces a short form of Myo95E (Figure 1C) (FlyBase, http://flybase.org/reports/FBgn0039157.html). The entire coding sequence of *Myo95E* is covered by two complementary DNA (cDNA) fragments, GH25580 and RE40416 (Rubin *et al.* 2000; Stapleton *et al.* 2002). RE40416 carries a *Myo95E* cDNA fragment encompassing its 5′ region, which contains extra insertions. To construct pUAST-Myo95E-RB, we first removed a 17-bp insertion in RE40416. Two fragments were amplified by PCR, using a T7 and T3 primer in conjunction with the gene-specific primers 5′-GGGAGATCCAATGGGAACCC GTATAACGGACCCTATC-3′ and 5′-GATAGGGTCCGTTATACG GGTTCCCATTGGATCTCCC-3′, respectively, with RE40416 as a template. Using these two PCR products as templates, the fragment from which the extra insertion was removed was amplified by PCR with T7 and T3 primers. This fragment (the modified RE40416) was digested by *Eco*RI and *Bam*HI and subcloned into the pGEM7 vector. The modified RE40416 was digested with *Eco*RI and *Sac*I, and GH22580 was digested with *Xho*I and *Sac*I. These fragments were then subcloned into the *Eco*RI and *Xho*I sites of pBluescript SK(−) to generate the full-length Myo95E-RB fragment. Myo95E-RD was a variant of Myo95E-RB containing a 60-bp deletion. To obtain the 5′ fragment of the *Myo95E-RD* cDNA, two fragments were first amplified by PCR with the T7 and pM001 primers (BDGP, http://www.fruitfly.org/about/methods/pOT2vector.html) in conjunction with the gene-specific primers, 5′-TCCACAAATGCCTAC GACCAGTGAAGGGAATGCCAAATCGGCATTCCCGCCACGTGC GCCAGGCACTCG-3′ and 5′-TTCCCTTCACTGGTCGTAGGCA TTTGTGGAGTTTATATCGTGTCGCCCGCGAGGAGTATCGG TCC-3′, using the cDNA of GH25580 as a template. Using these two PCR products as templates, PCR was again performed with the T7 and pM001 primers. The resulting PCR fragment (the modified GH25580) was subcloned into pBluescript SK(−), as described above. The modified RE40416 and GH25580 fragments were subcloned into the *Eco*RI and *Xho*I sites of pBluescript SK(−) to generate the full-length Myo95E-RD fragments, as described above. After sequence confirmation, the Myo95E-RB and Myo95E-RD fragments were subcloned into the *Eco*RI and *Xho*I sites of the pUAST vector (Brand and Perrimon 1993).

To construct pUAST-Myo95E-RF, RE40416 (obtained from the *Drosophila* Genomics Resource Center), which includes the cDNA for the entire coding sequence for *Myo95E-RF*, was digested by *Eco*RI and *Bam*HI. The full-length *Myo95E-RF* cDNA was cloned into the *Eco*RI and

*Bam*HI sites of BluescriptII SK(−). This construct was digested by *Eco*RI and *Not*I, and the full-length *Myo95E-RF* cDNA was cloned into the *Eco*RI and *Not*I sites of the pUAS-TattB vector (Bischof *et al.* 2007).

UAS-Myo95E-RB-FLAG encodes a full-length Myo95E-PB protein with a FLAG (DYKDDDDK) tag at the C terminus (Hopp *et al.* 1988). For this construct, a *Myo95E-RB* cDNA fragment was amplified by PCR with two primers, 5′-CACCGAATT CATGGAGCAGGAAATCGGCA-3′ and 5′-CACCCTCGAGTCACT TATCGTCATCGTCCTTGTAATCCACAATTATCTCCATGC GGTTCG-3′, containing the FLAG coding sequence, using the *Myo95E-RD* cDNA fragment as a template. The resulting PCR fragment was subcloned into the *Eco*RI and *Xho*I sites of pUAST.

UAS-Myo61F-mRFP encodes a full-length Myo61F protein tagged with a monomeric RFP (mRFP) at the C terminus (Campbell *et al.* 2002). For this construct, a full-length *Myo61F* cDNA was amplified by PCR, using a full-length *Myo61F* cDNA as a template (Hozumi *et al.* 2006) with the primers 5′-GGG GTACCTTGCGTTCCAATGATAACTAGATGG-3′ and 5′-CCGGA ATTCCTGACACATCCTCCAGAGAA-3′. An *mRFP* cDNA fragment was also obtained by PCR, using pRSET-mRFP1 (gift of A. Miyawaki, RIKEN, Wako, Saitama, Japan) as a template with the primers 5′-GGGGTACCATGGCCTCCTCCGAGGACGT CATC-3′ and 5′-TTCGAATTCTTAGGCGCCGG-3′. The two fragments were digested with *Eco*RI and *Kpn*I and subcloned into the *Eco*RI site of pBluescript SK(−). After sequence confirmation, these fragments were subcloned into the *Eco*RI and *Not*I sites of pUAST.

To generate the *pChs-Act5C-Gal4* construct, a fragment of the *Actin 5C* proximal promoter was amplified from the Canton-S genome by PCR, using the primers 5′-AGAATT CACGCCCTAAAACACCAGATCATCC-3′ and 5′-TGGTACCG CACGGTTTGAAAGGAATGACTGG-3′. The PCR product was subcloned into the *Eco*RI and *Kpn*I sites of the pChs-Gal4 vector (provided by the *Drosophila* Genomics Resource Center).

To construct pUAST-mGFP and pUAST-mRFP, the cDNAs for mGFP and mRFP were amplified by PCR from pUAST-Myo31DF-mGFP and pUAST-Myo61F-mRFP, respectively. Primers 5′-GGAATTCAACCAAACATGGTGAGCAAGGGCG AGGAG-3′ and 5′-GGACTAGTTTACTTGTACAGCTCGTCC ATGCC-3′ were used to amplify mGFP, and 5′-GGAATTCAAC CAAACATGGCCTCCTCCGAGGACGTCATC-3′ and 5′-GGACTA GTTTAGGCGCCGGTGGAGTGGCGG-3′ were used to amplify mRFP. The resulting fragments were subcloned into the *Eco*RI and *Spe*I sites of pBluescript SK(−). After sequence confirmation, these fragments were subcloned into the *Eco*RI and *Not*I sites of the pUASTattB vector (Bischof *et al.* 2007).

These constructs were used for germline transformation using standard protocols (Spradling 1986; Bischof *et al.* 2007) and/or for transfection into *Drosophila* Schneider 2 (S2) cells as described below (Cherbas and Cherbas 2000).

Generation of novel mutant alleles of Myo61F and Myo95E

To generate a novel mutant allele of *Myo61F*, we used imprecise excision of the *P* element inserted in the w^{1118};; $P\{EP\}Myo61F^{EP3325a}$ $P\{EP\}Myo61F^{EP3325b}$ line. First, we removed *P{EP}3325b* inserted at the cytological position of 86E18 by recombination. w^{1118};; $P\{EP\}Myo61F^{EP3325a}$ $P\{EP\}Myo61F^{EP3325b}$ virgin females were mated with w^{1118};; ru^1 h^1 st^1 ry^{506} e^1 males. The F_1 females (w^{1118};; $P\{EP\}Myo61F^{EP3325a}$ $P\{EP\}Myo61F^{EP3325b}$/ ru^1 h^1 st^1 ry^{506} e^1) were mated with w^{1118};; ru^1 h^1 st^1 ry^{506} e^1 males again, and the F_2 males (w^{1118};; $P\{EP\}Myo61F^{EP3325a}$ ry^{506} e^1/ ru^1 h^1 st^1 ry^{506} e^1) were balanced with *TM3*, $P\{ry^{+t7.2} = ftz\text{-}lacZ.ry^{+}\}TM3$, Sb^1 *ry** to generate stocks. The presence of $P\{EP\}Myo61F^{EP3325a}$ and absence of $P\{EP\}Myo61F^{EP3325b}$ were checked by PCR with the appropriate primers. $P\{EP\}Myo61F^{EP3325a}$ was inserted 2460 bp upstream of the presumptive initiation codon of *Myo61F-PA* and 750 bp upstream of the first exon in *CG9184*. The *CG9184* locus is present in the second intron of *Myo61F*. *H{PDelta2-3}HoP8* y^1 *w** virgin females, providing P transposase, were mated with w^{1118};; $P\{EP\}Myo61F^{EP3325a}$ ry^{506} e^1 males. The F_1 males (*H{PDelta2-3}HoP8* y^1 w*/ Y;; $P\{EP\}Myo61F^{EP3325a}$ ry^{506} e^1/ +) were mated with w^{1118};; Dr^1/*TM3*, $P\{ry^{+t7.2} = ftz\text{-}lacZ.ry^{+}\}TM3$, Sb^1 *ry** virgin females. The F_2 males (w^{1118}/ Y;; $P\{EP\}Myo61F^{EP3325a}$ ry^{506} e^1/*TM3*, $P\{ry^{+t7.2} = ftz\text{-}lacZ.ry^{+}\}TM3$, Sb^1 *ry**) were individually balanced to generate stocks. For each stock, genomic DNA was extracted from single flies, and potential deletions in the *Myo61F* locus were detected by PCR with the primers 5′-GATCGATCA AGCACCGTT-3′ and 5′-CGAAGTACTCCACAGGTATC-3′. We isolated a stock in which a part of the *Myo61F* locus was deleted and used it as a *Myo61F* null allele ($Myo61F^1$) (Figure 1B). $Myo61F^1$ has a 3454-bp deletion, which removes the putative initiation codon and the region encoding the ATP-binding site in all the Myo61F isoforms (Myo61F-PA, -PB, -PC, and -PD; Figure 1B). The deletion uncovers from nucleotide 1,323,560 to 1,327,013, by the numbering system used for the *Drosophila* genome in FlyBase (*Drosophila melanogaster* chromosome 3L, GenBank no. AE014296.5) (Adams *et al.* 2000). The $Myo61F^1$ ry^{506} e^1 chromosome was cleaned up by recombination with ru^1 h^1 st^1 ry^{506} e^1 and w^{1118} flies, and the markers were subsequently removed to establish the $Myo61F^1$ stock used in all the experiments.

Myo95E mutant alleles were also induced by imprecise excision of a *P* element. $P\{EPgy2\}Myo95E^{EY22671}$ carries a *P* element inserted 450 bp upstream of the putative initiation codon shared by all the alternative splicing products of *Myo95E* (*Myo95E-RB*, *-RD*, *-RE*, *-RF*, *-RG*, and *-RJ*). *w**; Dr^1/*TMS*, *P{Delta2-3}99B* virgin females, providing P transposase, were mated with $P\{EPgy2\}Myo95E^{EY22671}$/TM3, Sb^1 Ser^1 males. The F_1 males (*w**/Y;; $P\{EPgy2\}Myo95E^{EY22671}$/*TMS*, *P{Delta2-3}99B*) were mated with *w**; *TM3*, $P\{ry^{+t7.2} = ftz\text{-}lacZ.ry^{+}\}TM3$, Sb^1 *ry**/*TM6B*, *P{iab-2(1.7)lacZ}6B*, Tb^1 virgin females. The F_2 males (w^{1118}/Y;; $P\{EPgy2\}Myo95E^{EY22671}$/*TM3*, $P\{ry^{+t7.2} = ftz\text{-}lacZ.ry^{+}\}TM3$, Sb^1 *ry** or w^{1118}/Y;; $P\{EPgy2\}Myo95E^{EY22671}$/*TM6B*, *P{iab-2(1.7)lacZ}6B*, Tb^1) were individually balanced to establish stocks. For each stock, genomic DNA was extracted from single flies,

and deletions in the *Myo95E* locus were detected by PCR with the primers 5′-TAGGTTTCCACGTTGTCGTC-3′ and 5′-CTGCGGGAAATGCTTAAGAAG-3′. Two lines in which part of the *Myo95E* locus was removed were obtained and used as null alleles of *Myo95E* (*Myo95E*^{1} and *Myo95E*^{2}) (Figure 1C). *Myo95E*^{1} and *Myo95E*^{2} contain 2893- and 2118-bp deletions in the *Myo95E* locus, respectively, which remove the putative initiation codon and the region encoding the ATP-binding site in all the Myo95E isoforms (Myo95E-PB, -PD, -PE, -PF, -PG, and -PJ) (Figure 1C). The deletions in *Myo95E*^{1} and *Myo95E*^{2} uncover the nucleotides from 24,161,480 to 24,158,588 and from 24,161,480 to 24,159,363, respectively, by the numbering system used for the *Drosophila* genome in FlyBase (*D. melanogaster* chromosome 3R, GenBank no. AE014297.3) (Adams *et al.* 2000). The chromosome carrying *Myo95E*^{1} was cleaned up by recombination with w^{1118} and se^{1} ss^{1} k^{1} e^{s} ro^{1}.

A chromosome carrying both *Myo61F*^{1} and *Myo95E*^{1} was generated by recombination. The presence of deletions at these loci was confirmed by PCR as described above.

Whole-mount in situ hybridization

Canton-S embryos were dechorionated with 50% bleach, fixed with 4% paraformaldehyde, and devitellinized by 100% methanol. They were rehydrated and washed with phosphate-buffered saline containing 0.1% Tween 20 (PBStw) and then incubated in PBStw containing 10 μg/ml proteinase K for 3 min at 25°, washed with PBStw, and fixed with 4% paraformaldehyde for 20 min at 25°. The embryos were washed again with PBStw and then hybridized with digoxygenin-labeled RNA probes diluted with hybridization buffer (50% formamide, 5xSSC, 1 mg/ml tRNA, 50 μg/ml heparin, 0.1% tween) at 60° overnight. They were then washed with PBStw and incubated in 0.1% blocking reagent (Roche) for 1 hr at 25°. Anti-digoxygenin antibody labeled with alkaline-phosphatase (Roche, 1:7000) was added, and then the embryos were incubated for 1 hr at 25° and washed with PBStw. The alkaline-phosphatase activity was detected by Nitro blue tetrazolium chloride/5-Bromo-4-chloro-3-indolyl phosphate (NBT/BCIP) (Roche). The embryos were then mounted in 90% glycerol and analyzed with an Axioskop2 plus (Zeiss, Thornwood, NY). *Myo31DF*, *Myo61F*, and *Myo95E* cDNAs were used as templates for RNA probes prepared using a DIG RNA-labeling kit (Roche).

Real-time PCR

Total RNA was isolated from 10 pupae (23–25 hr after pupation) of wild-type or the *Myo61F*^{1} homozygote, using Isogen (Nippon Gene, Tokyo), and 1 μg of each RNA sample was used for cDNA synthesis with the PrimeScript RT reagent Kit with genomeDNA Eraser (Takara), according to the product manual. The amount of *CG9134* transcript was normalized to that of a housekeeping gene, *Glyceraldehyde 3 phosphate dehydrogenase 1* (*Gapdh1*) (Miyashita *et al.* 2012). The primers used to amplify *CG9134* were 5′-GGA GAGTGACTGCGATTGGTTTG-3′ and 5′-TGTTGCTGCTTT TCGGTCCTG-3′. The primers used to amplify *Gapdh1* were 5′-TTCAGCGACACCCATTCGTC-3′ and 5′-TACCACGAGAT TAGCTTGACGAAC-3′. Quantitative PCR was performed using SYBR Premix Ex Taq II (Takara) and the Applied Biosystems (Foster City, CA) 7300 Real Time PCR System according to the product manuals.

Immunohistochemistry

Antibody staining of the embryo, larval midgut, and S2 cells was performed as described previously (Ashburner *et al.* 1989). The primary antibodies used were mouse anti-αSpectrin [Developmental Studies Hybridoma Bank (DSHB), 1:25], mouse anti-Elav (DSHB, 1:100), mouse anti-Fas2 (DSHB, 1:10), rat anti-GFP (Nacalai Tesque, 1:500), rabbit anti-RFP (Medical & Biological Laboratories, Nagoya, Japan, 1:500), and mouse anti-FLAG M2 [Sigma (St. Louis), 1:1000]. The secondary antibodies used were Cy3-conjugated anti-mouse IgG (Jackson ImmunoResearch, 1:500), Alexa^{488}-conjugated anti-mouse IgG [Molecular Probes (Eugene, OR), 1:500], Cy3-conjugated rabbit IgG (Jackson ImmunoResearch, 1:500), and Alexa^{488}-conjugated anti-rat IgG (Molecular Probes, 1:500). We used rhodamine-, Alexa^{488}-, and Alexa^{633}-phalloidin to stain F-actin (Molecular Probes, 1: 35).

Stained embryos and larval gut tissues were mounted in 90% glycerol and analyzed with an Axioskop2 plus (Zeiss), LSM 5 PASCAL (Zeiss), or ECLIPSE Ti (Nikon, Garden City, NY). The images were processed with a Ziess LSM Image Browser, a Nikon EZ-C1 viewer, Adobe Photoshop CS4, and Adobe Illustrator CS6.

Analyses of the LR asymmetry of the embryonic gut and male genital plate

Following embryo fixation with 4% paraformaldehyde, the handedness of each section of the embryonic gut, the foregut (fg), the anterior midgut (amg), the posterior midgut (pmg), and the hindgut (hg) (see Figure 3A) was scored at stages 14–16, 16, 16, and 13–16, respectively, with an Axioskop2 plus. The genotypes of the embryos were determined with blue-balancers *CyO*, *P{en1}wg*^{en11} and *TM6B*, *P{iab-2(1.7)lacZ}6B*, *Tb*^{1}, after β-galactosidase staining according to a standard protocol (O'Kane 1998). The following embryos were analyzed: (1) Canton-S, (2) *Myo31DF*^{L152}/*Myo31DF*^{L152}, (3) *Myo61F*^{1}/*Myo61F*^{1}, (4) *Myo95E*^{1}/*Myo95E*^{1}, (5) *Myo31DF*^{L152}/*Myo31DF*^{L152}; *Myo61F*^{1}/*Myo61F*^{1}, (6) *Myo31DF*^{L152}/*Myo31DF*^{L152}; *Myo95E*^{1}/*Myo95E*^{1}, (7) *Myo61F*^{1} *Myo95E*^{1}/*Myo61F*^{1} *Myo95E*^{1}, (8) *Myo31DF*^{L152}/*Myo31DF*^{L152}; *Myo61F*^{1} *Myo95E*^{1}/*Myo61F*^{1} *Myo95E*^{1}, (9) *UAS-Myo95E-RB/da-GAL4*, (10) *UAS-Myo95E-RD/+*; *da-GAL4/+*, (11) *UAS-Myo95E-RF/+*; *da-GAL4/+*, (12) *UAS-Myo95E-RB/byn-GAL4*, (13) *UAS-Myo95E-RD/+*; *byn-GAL4/+*, (14) *UAS-Myo95E-RF/+*; *byn-GAL4/+*, (15) *UAS-Myo95E-RB/24B-GAL4*, (16) *UAS-Myo95E-RD/+*; *24B-GAL4/+*, (17) *UAS-Myo95E-RF/+*; *24B-GAL4/+*, (18) *Myo31DF*^{L152}/*Myo31DF*^{L152}; *da-GAL4/+*, (19) *Myo31DF*^{L152}, *UAS-Myo61F/Myo31DF*^{L152}; *da-GAL4/+*, and (20) *Myo31DF*^{L152}, *UAS-Myo95E-RB/Myo31DF*^{L152}; *da-GAL4/+*.

The direction of the male genitalia rotation was determined from the looping direction of the spermiduct, which attaches to the male genital plate and coils around the hindgut (Speder *et al.* 2006). The wild-type rotational direction was designated as dextral and the reversed direction as sinistral. The rotational extent (0°–360°) was determined by positions of the penis and anus. Flies with each of the genotypes indicated below were obtained from three separate vials, and the genitalia of 30 flies from each vial were scored. The average frequency (percentage) of individuals exhibiting genitalia rotation angles every 180° was calculated. The male genital plate images were captured with a VHX-100 (Keyence). Male flies with the following genotypes were analyzed: (1) Canton-S, (2) *Myo31DF^{K2}/Myo31DF^{K2}*, (3) *Myo61F^{1}/Myo61F^{1}*, (4) *Myo95E^{1}/Myo95E^{1}*, (5) *Myo31DF^{K2}/Myo31DF^{K2}*; *Myo61F^{1}/Myo61F^{1}*, (6) *Myo31DF^{K2}/Myo31DF^{K2}*; *Myo61F^{1}/Df(3L)BSC250*, (7) *Myo31DF^{K2}/Myo31DF^{K2}*; *Myo95E^{1}/Myo95E^{1}*, (8) *Myo61F^{1} Myo95E^{1}/Myo61F^{1} Myo95E^{1}*, (9) *Myo31DF^{K2}/Myo31DF^{K2}*; *Myo61F^{1} Myo95E^{1}/Myo61F^{1} Myo95E^{1}*, (10) *Myo31DF^{K2} ptc-GAL4/+*, (11) *Myo31DF^{K2} ptc-GAL4/Myo31DF^{L152}*, (12) *Myo31DF^{K2} ptc-GAL4/Myo31DF^{K2}*, (13) *Myo31DF^{K2} ptc^{16}/Myo31DF^{K2}*, (14) *Myo31DF^{K2}/Myo31DF^{K2}*; *hh-GAL4/+*, (15) *ptc-GAL4/UAS-Myo31DF-GFP*, (16) *Myo31DF^{K2} ptc-GAL4/UAS-Myo31DF-GFP*, (17) *Myo31DF^{K2} ptc-GAL4/Myo31DF^{L152}*, *UAS-Myo31DF-GFP*, (18) *ptc-GAL4/UAS-Myo61F*, (19) *Myo31DF^{K2} ptc-GAL4/UAS-Myo61F*, (20) *Myo31DF^{K2} ptc-GAL4/Myo31DF^{L152}*, *UAS-Myo61F*, (21) *ptc-GAL4/UAS-Myo95E-RB*, (22) *Myo31DF^{K2} ptc-GAL4/UAS-Myo95E-RB*, and (23) *Myo31DF^{K2}*, *ptc-GAL4/Myo31DF^{L152}*, *UAS-Myo95E-RB*.

Hatching and survival rate analysis

The hatching and survival rates of wild-type and class I myosin single, double, or triple mutants were measured as follows. For hatching rates, 50 embryos were collected and maintained at 25° for 24 hr, and the number of hatched larvae was counted. To obtain *Myo95E^{1}/Df(3R)Excel6198* flies, *Myo95E^{1}* homozygous females were mated with *Df(3R)Excel6198/TM3*, *P{w[+mC]=sChFP}3* males. In other experiments, to remove the maternal contribution, the progenies of females homozygous for the single, double, and triple mutants of *Myo31DF*, *Myo61F*, or/and *Myo95E^{1}* were obtained.

For survival rates from the first-instar larvae to adult, 50 first-instar larvae were cultured in vials with the standard medium at 25°, and the number of eclosed flies was counted 14 days later. For adult survival rates, 20 adult flies of each genotype were collected 0–8 hr after eclosion. Males and females were distinguished among these flies, and they were transferred separately into standard medium. Surviving flies were counted when the flies were transferred into new culture medium every 3 days. During this experiment, flies were kept at 25°. For both the hatching and the survival analyses, five experiments were performed independently, and the results were statistically analyzed. Embryos and larvae with the following genotypes were analyzed: (1) Canton-S, (2) *Myo31DF^{L152}/Myo31DF^{L152}*, (3) *Myo61F^{1}/Myo61F^{1}*, (4) *Myo95E^{1}/Myo95E^{1}*, (5) *Myo31DF^{L152}/Myo31DF^{L152}*; *Myo61F^{1}/Myo61F^{1}*, (6) *Myo31DF^{L152}/Myo31DF^{L152}*; *Myo95E^{1}/Myo95E^{1}*, (7) *Myo61F^{1} Myo95E^{1}/Myo61F1 Myo95E^{1}*, and (8) *Myo31DF^{L152}/Myo31DF^{L152}*; *Myo61F^{1} Myo95E^{1}/Myo61F^{1} Myo95E^{1}*.

Subcellular localization analysis using S2 cells

The *Drosophila* S2 cells were cultured in M3 insect medium (Sigma) with 10% fetal bovine serum (Biowest). S2 cells were cotransfected with *pChs-Act5C-Gal4* and *pUAST-Myo31DF-mEGFP*, *pUAST-Myo61F-mRFP*, *pUAST-Myo95E-RB-FLAG*, *pUAST-mEGFP*, or *pUAST-mRFP* or combinations of any two, using Cellfectin (Invitrogen, Carlsbad, CA). One to 2 days after transfection, the cells were plated on glass coverslips coated with concanavalin A (Sigma), fixed with 4% paraformaldehyde, stained with antibodies and fluorescently labeled phalloidin as described above, mounted in 90% glycerol, and analyzed with an Axioskop2 plus and LSM 5 PASCAL. The captured images were processed with a Ziess LSM Image Browser and Adobe Photoshop CS4.

Results

Generation of novel mutant alleles of Myo61F and Myo95E

In this study, we generated novel mutant alleles of *Myo61F* and *Myo95E*, using a method involving imprecise excision of *P* elements (Grigliatti 1998). To induce deletions, we mobilized the *P*-elements *EP3325b* and *EY22671* inserted in the vicinity of the *Myo61F* and *Myo95E* loci, respectively (Figure 1, B and C). We isolated one mutant allele of *Myo61F*, *Myo61F^{1}*, and two mutant alleles of *Myo95E*, *Myo95E^{1}* and *Myo95E^{2}* (Figure 1, B and C).

The *Myo61F* gene produces four alternative transcripts, *Myo61F-RA*, *-RB*, *-RC*, and *-RD* (Figure 1B) (FlyBase, http://flybase.org/reports/FBgn0010246.html). These four alternative splicing products encode Myo61F isoforms that have all of the characteristic structures of class I myosins, such as the ATP- and actin-binding sites, IQ motifs, and TH1 domains (Coluccio 1997; Barylko *et al.* 2000). Our sequencing analysis of the *Myo61F^{1}* locus revealed that it lacked the genomic region encompassing the putative initiation codons for all four alternative splicing products as well as exons encoding portions of the motor domains, including the ATP-binding site (Figure 1B). Since the ATP-binding site is necessary for the motor activity of myosin family proteins (Molloy *et al.* 1995; Fan *et al.* 2012), this mutant was predicted to function as null alleles. In addition, our real-time PCR analysis revealed that the transcription efficiency of the *CG9184* gene, which is located in the second intron of *Myo61F*, was not affected in the *Myo61F^{1}* homozygote (Supporting Information, Figure S1). We examined the amount of *CG9184* messenger RNA (mRNA) at the pupal stage, because our analysis described below revealed that *Myo61F* functions in the rotation of the male genitalia, which occurs at this stage. We found that the mRNA level of *CG9184* was not

significantly different between wild-type (1.0 ± 0.22) and the *Myo61F*^{1} homozygote (1.37 ± 0.31) (Figure S1), indicating that the *CG9184* expression was intact in this mutant.

The *Myo95E* gene produces six alternative transcripts, *Myo95E-RB*, *-RD*, *-RE*, *-RF*, *-RG*, and *-RJ* (Figure 1C) (FlyBase, http://flybase.org/reports/FBgn0039157.html). Among them, *Myo95E-RB*, *-RD*, *-RE*, and *-RJ* encode long isoforms and *Myo95E-RF* and *-RG* encode short forms of Myo95E. The head region of all six Myo95E isoforms has an atypical insertion (Figure 1A) (Tzolovsky *et al.* 2002). Genome sequencing analyses showed that the *Myo95E*^{1} and *Myo95E*^{2} loci lacked the genomic region containing the putative initiation codon for all six alternative splicing products from the *Myo95E* locus (Figure 1C). These six alternative splicing products also lost exons encoding portions of the motor domain, including part of the ATP-binding site (Figure 1C). These findings indicate that *Myo95E*^{1} and *Myo95E*^{2} are null alleles of *Myo95E*. We used the *Myo95E*^{1} allele in subsequent studies, because it had a larger deletion than *Myo95E*^{2} (Figure 1C).

Myo31DF or *Myo61F* homozygous mutant flies were previously reported to be viable and fertile (Hozumi *et al.* 2006; Speder *et al.* 2006; Hegan *et al.* 2007). Our finding that the *Myo61F*^{1} or *Myo95E*^{1} homozygotes were also viable and fertile (data not shown) combined with the earlier data suggests that all class I myosins are dispensable for survival in *Drosophila*, if their functions are disrupted separately. In this study, we further measured the hatching and survival rates of the single, double, and triple mutants. To remove the effect of maternal contributions of these genes, only the progenies of females homozygous for the single, double, and triple mutants were scored. The hatching rates and survival rates from first-instar larvae to adult (L1 to adult) of *Myo31DF*^{L152} (null mutant of *Myo31DF*) (Hozumi *et al.* 2006), *Myo61F*^{1}, or *Myo95E*^{1} single mutants were similar to those of wild type (Figure S2, A and B). We further characterized the *Myo95E*^{1} allele as the first reported mutant of *Myo95E*. The hatching rate of embryos that were *trans*-heterozygotes for a deletion mutant uncovering the *Myo95E* locus [*Df(3R)Exel6198*] and the *Myo95E*^{1} mutant (obtained from *Myo95E*^{1} homozygous females) was similar to that of the *Myo95E*^{1} homozygote obtained from *Myo95E*^{1} homozygous females (not significant by *t*-test, Figure S3) (Parks *et al.* 2004). This result supported the idea that *Myo95E*^{1} is a null allele of *Myo95E*. We then analyzed in detail the structures of the embryonic and adult organs of the *Myo95E*^{1} homozygotes obtained from *Myo95E*^{1} homozygous females, but observed no abnormalities (data not shown).

Furthermore, the double and triple mutants of *Myo31DF*^{L152}, *Myo61F*^{1}, and/or *Myo95E*^{1} were viable and fertile (data not shown), and their hatching rates and survival rates of L1 to adult were largely comparable to those of wild-type (Figure S2, A and B). However, certain mutant combinations showed some reduction (up to 50%) in their hatching and/or survival rate (Figure S2, A and B). In addition, the survival rates of adults were decreased in the single, double, and triple mutants (Figure S2C). These results demonstrated that class I myosins are not essential for survival itself, but are required for optimal hatching and survival rates, and thus are important mediators in *Drosophila*, at least under our experimental conditions.

Differential expression of Myo31DF, Myo61F, and Myo95E during embryogenesis

Myo31DF and *Myo61F* mRNAs and their protein products are detected in the gut epithelium and genital disc (Morgan *et al.* 1995; Hozumi *et al.* 2006; Speder *et al.* 2006; Petzoldt *et al.* 2012). To gain insight into the tissue-specific roles and functional redundancy of the three class I myosins in the LR asymmetric development of the embryonic gut, we analyzed their expression in embryos, using *in situ* hybridization. The *Drosophila* embryonic gut was divided into four sections, the fg, amg, pmg, and hg, as depicted clearly at stage 16 (see Figure 3A). *Myo31DF* mRNA was detected in the amg, pmg, hg, and salivary gland (sg) primordia (Figure 2, A and B) at stages 12–16 and in the dorsal ectoderm at stage 12 (data not shown). *Myo31DF* expression was also detected in the visceral mesoderm starting at stage 13 (Figure 2, B and C) and showed a strong signal in the presumptive region of the gastric caeca (gc) and the three constriction sites of the midgut (Figure 2, B and C). Thus, *Myo31DF* expression underwent dynamic changes during embryogenesis. The *Myo31DF* signal was not detected by the sense probe (Figure 2D), indicating that it was specific.

Myo61F expression was first detected at stage 12 in the amg, pmg, and stomatogastric nervous system (sns) (Figure 2E) and then in the trachea from stage 14 onward (Figure 2F). *Myo61F* expression continued until stage 16 (Figure 2G) and was not detected with the sense probe (Figure 2H).

Myo95E mRNA was specifically detected in the neuroblast (nb) at stage 12 (Figure 2I) and continued to be expressed in the central nervous system (CNS) throughout embryogenesis (Figure 2, J and K). This signal was also undetectable with the sense probe (Figure 2L).

In summary, except for the expression of *Myo31DF* and *Myo61F* in the amg and pmg, which form the prospective midgut epithelium, the three myosin I genes were expressed in different tissues during embryogenesis. Since *Myo95E* was specifically expressed in the embryonic CNS, we further examined the CNS and third-instar larval brain in the *Myo95E*^{1} homozygotes obtained from *Myo95E*^{1} homozygous females, by immunostaining with anti-Elav and anti-Fas2 antibodies. We did not find any obvious morphological defects in these organs (data not shown), suggesting that *Myo95E* was not required for the overall formation of the CNS; however, we cannot rule out the possibility that a redundant mechanism exists.

LR asymmetric development of the embryonic gut does not involve Myo61F or Myo95E

Our results showed that both *Myo31DF* and *Myo61F* were expressed in the amg and pmg, suggesting potential functional

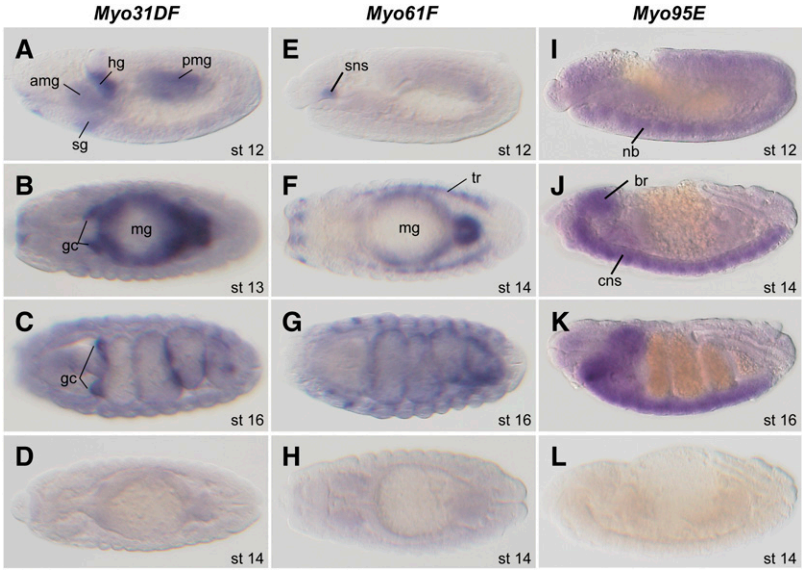

Figure 2 Differential expression of *Myo31DF*, *Myo61F*, and *Myo95E* transcripts during embryogenesis. (A–L) Whole-mount *in situ* hybridization of embryos stained with antisense (A–C) and sense (D) probes for *Myo31DF* mRNA, antisense (E–G) and sense (H) probes for *Myo61F* mRNA, and antisense (I–K) and sense (L) probes for *Myo95E* mRNA. Lateral (A, E, and I–L), dorsal (B, D, F, and H), and ventral (C and G) views of embryos are oriented with anterior to the left. amg, anterior midgut; br, brain; cns, central nervous system; gc, gastric caeca; hg, hindgut; mg, midgut; nb, neuroblast; pmg, posterior midgut; sg, salivary gland; sns, stomatogastric nervous system; tr, trachea. The embryonic stages are indicated at the bottom right.

redundancy during LR asymmetric development of the embryonic gut. Although the expression of *Myo95E* was predominantly detected in the CNS in embryos, it was possible that low levels of *Myo95E* contributed to the LR asymmetric development of the embryonic gut as well. Therefore, to determine the involvement of the class I myosins in this process, we examined the morphology of the embryonic gut in double and triple myosin I mutants.

Each section of the wild-type gut exhibits a directional LR asymmetric morphology, as shown previously and in Figure 3, A–C, which is genetically determined (Figure 3F) (Hayashi and Murakami 2001; Ligoxygakis *et al.* 2001). The pmg and hg exhibit an LR-reversed phenotype in ~80% of the $Myo31DF^{L152}$ homozygotes (Figure 3F) (Hozumi *et al.* 2006). However, the *Myo61F* and *Myo95E* single- and double-homozygous mutant embryos ($Myo61F^{1}/Myo61F^{1}$, $Myo95E^{1}/Myo95E^{1}$, and $Myo61F^{1}$ $Myo95E^{1}/Myo61F^{1}$ $Myo95E^{1}$) showed normal LR asymmetric development in all sections of the embryonic gut (Figure 3F). In addition, double- and triple-homozygous mutant flies carrying the *Myo31DF* mutant ($Myo31DF^{L152}/Myo31DF^{L152}$; $Myo61F^{1}/Myo61F^{1}$, $Myo31DF^{L152}/Myo31DF^{L152}$; $Myo95E^{1}/Myo95E^{1}$, and $Myo31DF^{L152}/Myo31DF^{L152}$; $Myo61F^{1}$ $Myo95E^{1}/Myo61F^{1}$ $Myo95E^{1}$) showed LR inversion in the pmg and hg with ~80% frequency, equivalent to the frequency of LR inversion in the $Myo31DF^{L152}$ homozygote (Figure 3, D–F). These results suggest that Myo61F and Myo95E do not play redundant roles with Myo31DF in LR asymmetric development in the embryonic gut and that Myo61F and Myo95E are not involved in the LR asymmetric development of this organ.

The overexpression of *Myo61F* in wild-type embryos results in LR inversion of the embryonic pmg and hg and the male genitalia (Hozumi *et al.* 2006, 2008; Petzoldt *et al.* 2012). We also reported that the ubiquitous overexpression of *Myo31DF* reverses the LR asymmetry of the fg and amg, whereas the *Myo31DF* loss-of-function mutant does not show LR inversion in these organs (Hozumi *et al.* 2006). In this study, to examine the potential activity of Myo95E in LR asymmetric development, we overexpressed *UAS-Myo95E-RB*, *UAS-Myo95E-RD*, and *UAS-Myo95E-RF* (Figure 1C). The first two produce long isoforms and the last one produces a short isoform of Myo95E (Figure 1C). These three transgenes were misexpressed under the control of *da-GAL4* (ubiquitous expression), *byn-GAL4* (gut specific), *24B-GAL4* (mesoderm), *ptc-GAL4* (male genitalia), and *Abd-B-GAL4* (male genitalia) (Brand and Perrimon 1993; Foronda *et al.* 2006; Suzanne *et al.* 2010). However, we did not observe LR asymmetry defects in any part of the embryonic gut or in genital disc rotation (Figure 3F, Figure 4G, and Figure S4). These results suggest that the misexpression of *Myo95E*, encoding the long or short isoforms, does not influence the LR asymmetric development of *Drosophila*.

We also overexpressed *Myo61F* and *Myo95E* in $Myo31DF^{L152}$ homozygous embryos, 70–80% of which exhibited LR inversion of the pmg and hg, as reported previously (Figure 3F). *Myo95E-RB* or *Myo95E-RD* overexpression did not affect the frequency of LR defects in the $Myo31DF^{L152}$ homozygous embryos (Figure 3F). However, unexpectedly, *Myo61F* overexpression increased the frequency of LR defects to 100% in $Myo31DF^{L152}$ homozygous embryos (Figure 3F). This result suggests that the sinistral activity of Myo61F was independent of Myo31DF. This finding prompted us to reconsider the previously proposed model suggesting that Myo61F does not have intrinsic sinistral activity, but rather acts as a negative regulator of Myo31DF (Hozumi *et al.* 2006; Petzoldt *et al.* 2012). However, despite the strong sinistral activity of overexpressed Myo61F, there was no detectable effect of the *Myo61F* loss-of-function mutation, even in combination with *Myo31DF* and/or *Myo95E* mutations, on the LR asymmetric development of the embryonic gut (Figure 3F).

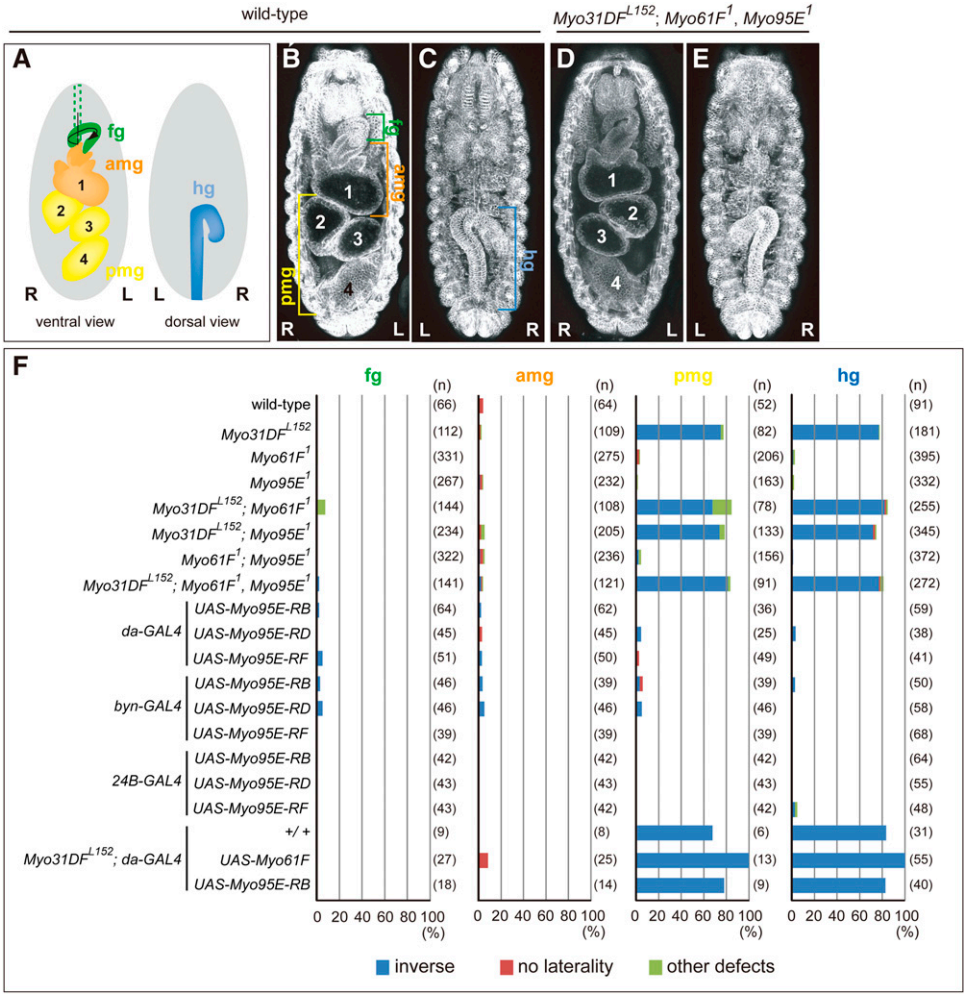

Figure 3 LR phenotypes of the embryonic gut associated with mutations and overexpression of *Myo31DF*, *Myo61F*, and *Myo95E*. (A) Diagram showing the LR asymmetric morphology of the embryonic gut viewed from the dorsal (right) and ventral (left) sides at late stage 16. The gut was divided into four parts, the foregut (fg), anterior midgut (amg), posterior midgut (pmg), and hindgut (hg). (B–E) Dorsal (C and E) and ventral (B and D) views of the wild-type (B and C) and *Myo31DF*^{L152}; *Myo61F*^{1} *Myo95E*^{1} homozygous (D and E) embryos at late stage 16, stained with an anti-α-Spectrin antibody. Anterior is up. Numbers indicate each chamber of the midgut. R, right; L, left. (F) Bar graphs showing the frequency of LR defects in each part of the embryonic gut in embryos with various genotypes, indicated at left. Blue, red, and green bars indicate LR inversion, no laterality, and other morphological defects, respectively. The number of embryos examined is indicated in parentheses at right.

Functional redundancy of Myo61F and Myo31DF in establishing LR asymmetry of the male genitalia

The male genital disc is another organ in which LR asymmetric development is studied extensively (Speder *et al.* 2006; Suzanne *et al.* 2010; Kuranaga *et al.* 2011; Petzoldt *et al.* 2012; Coutelis *et al.* 2013). The male genitalia normally undergo a dextral 360° rotation during wild-type pupal development (Figure 4, A and B) (Suzanne *et al.* 2010). The 360° rotation results from two stepwise 180° rotations involving two ring-shaped domains of the A8 segment (Suzanne *et al.* 2010; Kuranaga *et al.* 2011). In contrast, *Myo31DF* mutant flies exhibit a sinistral (LR-inversed) rotation of this organ (Figure 4, A and C) (Speder *et al.* 2006; Suzanne *et al.* 2010). *Myo61F* overexpression in the A8 segment also causes LR inversion of the male genital disc rotation (Petzoldt *et al.* 2012). This observation is consistent with our previous finding that *Myo61F* overexpression antagonizes dextral LR asymmetric development in the pmg and hg (Hozumi *et al.* 2006), although Myo31DF is not a target of Myo61F in this process, as found above.

To analyze the rotational defects of male genitalia quantitatively, we first defined the dorsal and the ventral axis from the positions of the penis (ventral side) and anus (dorsal side) (Figure 4A). In wild-type, the ventral and dorsal sides were then defined as 0°/360° and 180°, respectively (Figure 4A). The LR direction of rotation was determined from the coiling orientation of the spermiduct, observed when the male abdomen was dissected (Figure 4A) (Speder *et al.* 2006). In dextral (right-handed) rotation, the left and right sides of the male genitalia were defined as 90° and 270°, respectively (Figure 4A). Conversely, in the sinistral (left-handed) rotation, the left and right sides of the male genitalia were defined as 270° and 90°, respectively (Figure 4A). In the genitalia of each male, a straight line connecting the penis and anus was defined, and the rotation angle required to position the penis at 0°/360° by either dextral or sinistral rotation was determined (Figure 4A). Based on this rotation angle and its direction, adult males were classified into seven categories, which were color coded (Figure 4, F and G, and Figure S4).

As reported previously, wild-type males showed the dextral 360° rotation with 100% frequency, while *Myo31DF*^{K2} homozygotes showed either the sinistral 180°–360° or the sinistral 360° rotation (Speder *et al.* 2006) (Figure 4F). Here,

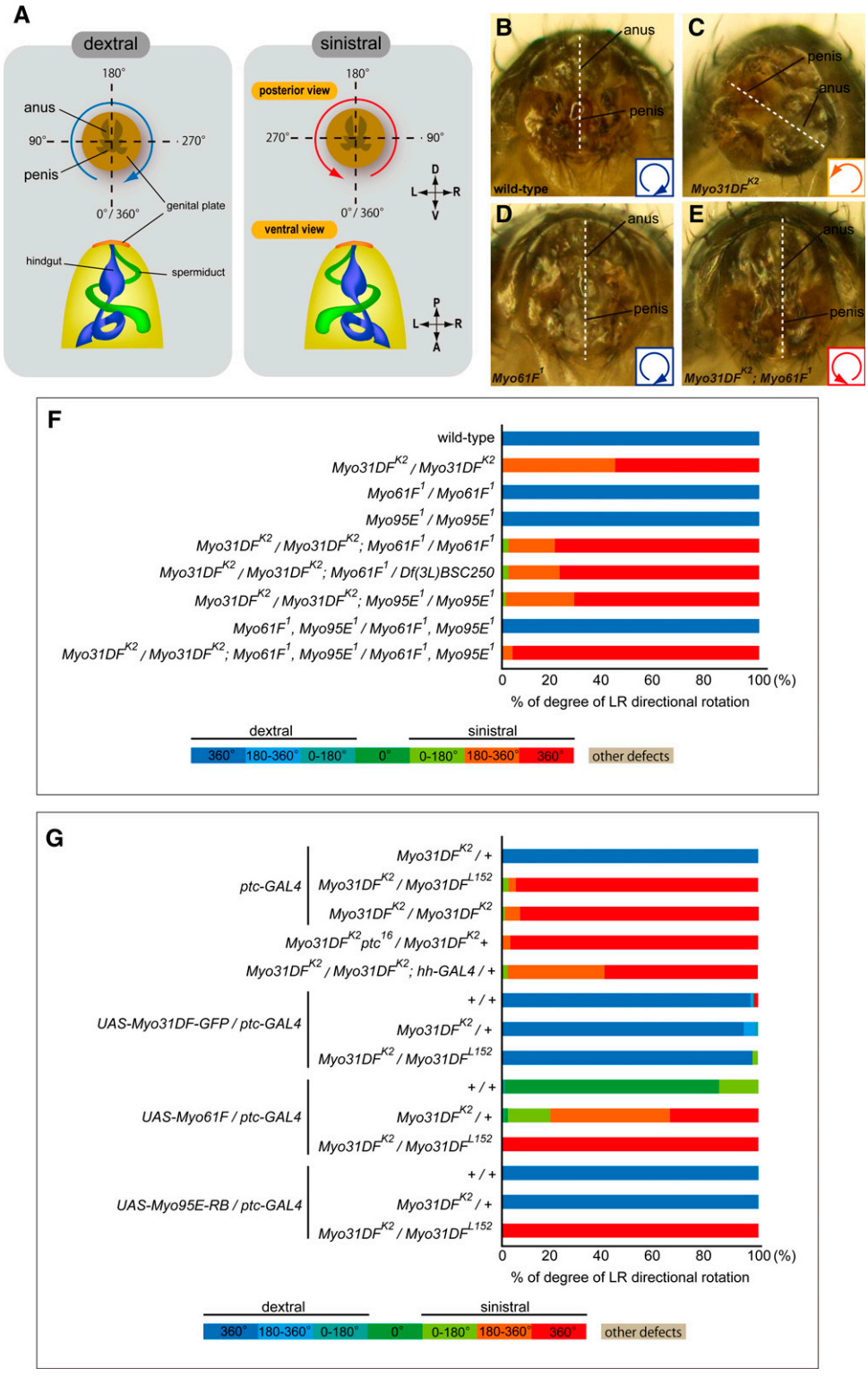

Figure 4 LR phenotypes of the male genitalia associated with mutations and overexpression of *Myo31DF*, *Myo61F*, and *Myo95E*. (A) Male genital plate of the wild-type (top left) and *Myo31F* homozygous mutant (top right) showing dextral (blue arrow) and sinistral (red arrow) rotations, respectively, viewed from the posterior during pupal stages. The spermiduct attached to the genital plate also showed dextral and sinistral looping around the hindgut in wild-type (bottom left) and *Myo31F* mutant homozygous flies (bottom right), respectively. A, anterior; D, dorsal; L, left; P, posterior; R, right; V, ventral. (B–E) Posterior views of the male genital plate of wild-type (B), $Myo31DF^{K2}$ homozygote (C), $Myo61F^{1}$ homozygote (D), and $Myo31DF^{K2}$; $Myo61F^{1}$ double-homozygote (E) flies. Dorsal is up. Insets at bottom right indicate the 360° dextral (blue), 180°–360° sinistral (orange), and 360° sinistral (red) rotations. White dotted lines indicate the midline of the genital plate. (F and G) Bar graphs showing the frequency (percentage) of dextral and sinistral rotation phenotypes observed in the male genital plate, color coded according to the categories shown at the bottom. Genotypes are indicated at left.

we showed that the $Myo61F^{1}$ or $Myo95E^{1}$ homozygote and the corresponding double homozygote showed the dextral 360° rotation with 100% frequency, as found in the wild-type (Figure 4, D and F), indicating that these mutations alone did not disrupt the LR asymmetric rotation. However, we found that $Myo31DF^{K2}/Myo31DF^{K2}$; $Myo61F^{1}/Myo61F^{1}$ and $Myo31DF^{K2}/Myo31DF^{K2}$; $Myo61F^{1}/Df(3L)BSC250$ males exhibited stronger sinistral rotation phenotypes, compared with that of the *Myo31DF* mutant homozygote ($P < 0.01$, *Z*-test; Figure 4F). This enhancing effect was also observed in the triple-homozygous, $Myo31DF^{K2}$; $Myo61F^{1}$; $Myo95E^{1}$ males ($P < 0.01$, *Z*-test; Figure 4F). These results suggest that the *Myo61F* mutation enhanced the sinistral rotation phenotype associated with the *Myo31DF* mutation. In contrast,

the sinistral rotation phenotype was not modified in the *Myo31DF*^{K2}; *Myo95E*^{1} homozygous males (no statistical significance; Figure 4F). This functional redundancy of Myo31DF and Myo61F was tissue specific, as it was not observed in the LR asymmetric development of the embryonic pmg and hg (Figure 3F).

Next, we examined whether the overexpression of *Myo31DF*, *Myo61F*, or *Myo95E* affects the LR rotation of the male genitalia in the wild-type or *Myo31DF* mutant background. Their expression was driven by *ptc-GAL4*, which expresses *GAL4* in the entire A8 and the anterior part of the A9 and A10 segments (Suzanne *et al.* 2010). As a control, *ptc-GAL4* was introduced into the wild-type (+/+), *Myo31DF*^{K2}/+, *Myo31DF*^{K2}/*Myo31DF*^{K2}, or *Myo31DF*^{K2}/*Myo31DF*^{L152} backgrounds without any *UAS* transgene. *Myo31DF*^{K2} *ptc-GAL4*/+ flies (*Myo31DF* heterozygotes) showed the complete dextral rotation, while *Myo31DF*^{K2} *ptc-GAL4*/*Myo31DF*^{L152} or *Myo31DF*^{K2} *ptc-GAL4*/*Myo31DF*^{K2} flies (*Myo31DF* homozygotes) primarily showed the complete sinistral rotation (Figure 4G). We noted that the penetrance of the sinistral rotation phenotype was higher in these flies than in the *Myo31DF*^{K2}/*Myo31DF*^{K2} flies, which did not carry *ptc-GAL4* (Figure 4, F and G). This enhancement of the sinistral rotation phenotype was probably due to *ptc*-GAL4, which is known to be a hypomorphic allele of *ptc* (Shyamala and Bhat 2002). On the other hand, the *hh-GAL4* line, which drives *GAL4* expression in the male genitalia, alone did not affect the sinistral rotation phenotype, suggesting that the influence of *ptc-GAL4* on this phenotype was specific (Figure 4G). This idea was further supported by our observation that *Myo31DF*^{K2} *ptc*^{16}/*Myo31DF*^{K2} flies showed a more severe sinistral rotation phenotype than *Myo31DF*^{K2}/*Myo31DF*^{K2} flies. *ptc*^{16} is a loss-of-function allele of *ptc* (Strutt *et al.* 2001). Therefore, in the following experiments, the baseline of the rotation phenotype was highly penetrant (>95%) complete sinistral rotation (Figure 4G).

We then overexpressed *Myo31DF-GFP*, *Myo61F*, and *Myo95E-RB* under the control of *ptc-GAL4* in wild-type (+/+), *Myo31DF*^{K2}/+, or *Myo31DF*^{K2}/*Myo31DF*^{L152} flies (Figure 4G). The overexpression of *Myo31DF-GFP* completely suppressed the sinistral rotation phenotype in *Myo31DF*^{K2}/*Myo31DF*^{L152} flies (Figure 4G). On the other hand, the overexpression of *Myo61F* resulted in no rotation and partial sinistral rotational phenotypes in wild-type and *Myo31DF*^{K2}/+ flies, respectively (Figure 4G). This result suggested that Myo31DF antagonizes the sinistral activity of *Myo61F* overexpression, as reported previously (Taniguchi *et al.* 2007). However, our loss-of-function analysis of *Myo31DF* and *Myo61F* showed that these two myosins function redundantly in dextral rotation of the male genital disc. Therefore, as found in the hindgut (Figure 3), it is likely that the sinistral activity of Myo61F is a neomorphic function associated with its overexpression.

In contrast, overexpression of *Myo95E-RB* did not affect the LR asymmetric rotation of the male genitalia in wild-type (+/+), *Myo31DF*^{K2}/+, or *Myo31DF*^{K2}/*Myo31DF*^{L152} flies (Figure 4G). Therefore, in our loss-of-function and overexpression analyses, we did not detect an effect of *Myo95E* in the LR asymmetric rotation of the embryonic gut or male genitalia.

Myo31DF, Myo61F, and Myo95E colocalize with F-actin in S2 cells and in larval midgut enterocytes

The head region of Myo95E has an atypical insertion (Figure 1A) (Tzolovsky *et al.* 2002). Therefore, we speculated that Myo95E may exhibit a different subcellular distribution from that of Myo31DF and Myo61F. The colocalization of Myo31DF-GFP and F-actin was previously reported in *Drosophila* S2 cells (Hozumi *et al.* 2006). Thus, we analyzed the subcellular localization of Myo61F-mRFP and Myo95E-PB-FLAG in S2 cells, in which F-actin was detected by phalloidin staining (Figure 5, A–A′′ and B–B′′). Myo61F-mRFP and Myo95E-PB-FLAG colocalized with F-actin in most of the cells overexpressing these proteins (Figure 5, A–A′′ and B–B′′). This colocalization pattern was similar to that of Myo31DF-GFP described previously (Hozumi *et al.* 2006). On the other hand, the mGFP and mRFP proteins, used as negative controls, did not show such colocalization with F-actin in any case examined, supporting the idea that the colocalization of these class I myosins with F-actin was specific (Figure 5, C–C′′). In a small population of cells (<20%) in which F-actin did not form aggregates, Myo61F-mRFP and Myo95E-RB-FLAG were evenly distributed in the cytoplasm (data not shown). Thus, in those cells, it was difficult to analyze the colocalization of F-actin with Myo61F and Myo95E. However, overall, our results were consistent with previously described interactions between class I myosins and F-actin.

We next studied the subcellular distribution of the three class I myosin proteins *in vivo*. Myo31DF and Myo61F are both known to be present in the apical brush border of the larval midgut enterocyte (Morgan *et al.* 1995). The apical brush border is composed of microvilli supported by F-actin bundles that protrude into the terminal web domain (Fath *et al.* 1993; Phillips and Thomas 2006) (Figure 5D). Protein delivery and recovery by endocytosis and exocytosis actively occur in the microvilli. The terminal web domain is a filamentous structure found in the most apical cytoplasmic region, in which F-actin bundles associated with the brush border are cross-linked by Spectrin and nonmuscle myosin II (Phillips and Thomas 2006). In the apical brush border, Myo31DF is enriched in the terminal web domain, and Myo61F is predominantly detected in the microvilli, and these expression regions overlap (Morgan *et al.* 1995). In this study, we compared the distribution of Myo95E-PB-FLAG with those of Myo31DF-mEGFP and Myo61F-mRFP in the enterocytes of the larval midgut overexpressing one of these three types of myosin I. F-actin in the apical brush border was detected by phalloidin staining (Figure 5, E′–G′ and E′′–G′′, magenta).

In our experiments, Myo31DF-mEGFP, Myo61F-mRFP, and Myo95E-RB-FLAG were all detected in the apical brush border, where F-actin was enriched (Figure 5, D and E–G′′).

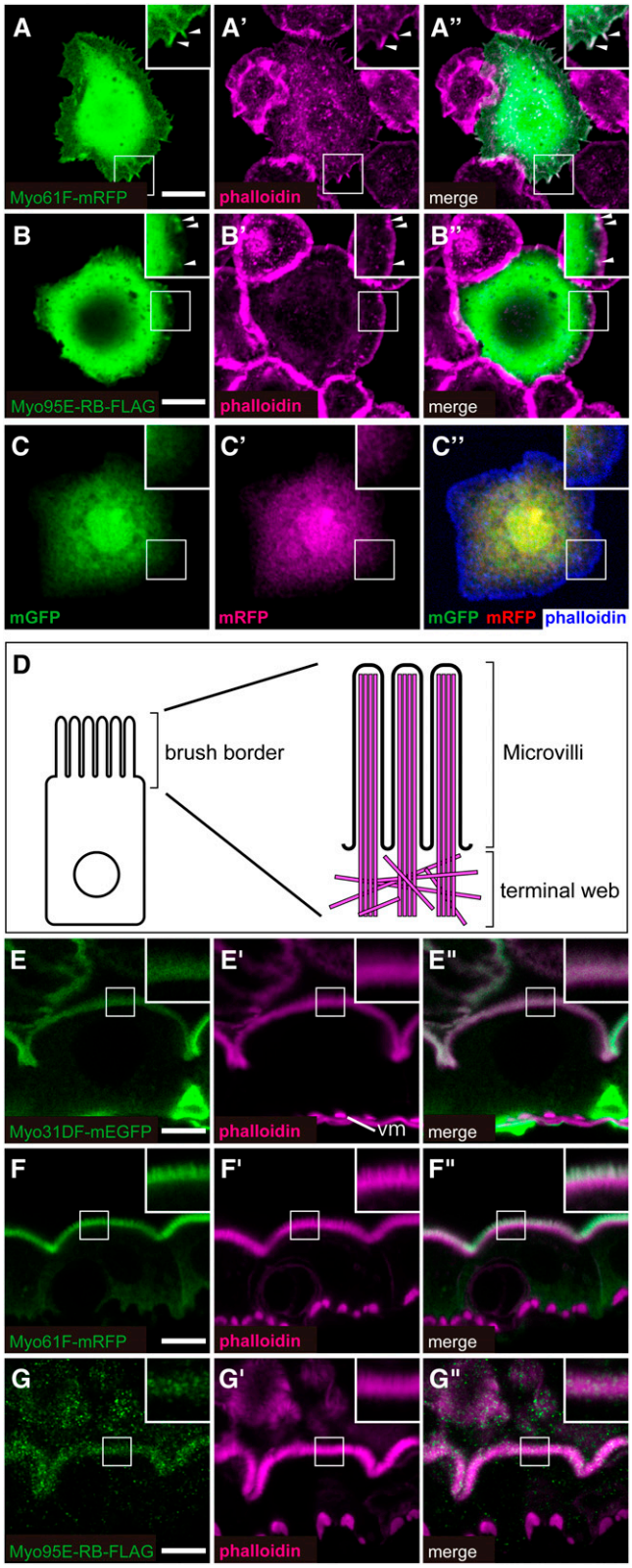

Figure 5 Subcellular localization of *Drosophila* class I myosin proteins. (A–C) Subcellular localization of Myo61F-mRFP (green in A and A′′), Myo95E-RB-FLAG (green in B and B′′), and control proteins mGFP (green in C and C′′) and mRFP (magenta in C′ and C′′) in *Drosophila* S2 cells. F-actin (magenta in A′, A′′, B′, and B′′ and blue in C′′) was stained by fluorescently labeled phalloidin. Insets in A–C′′ are high magnifications of the areas shown by white squares, and arrowheads in the insets (A–B′′) indicate the colocalization of Myo61F-mRFP or Myo95E-RB-FLAG with F-actin. A′′, B′′, and C′′ are merged images of A and A′, B and B′, and C and C′, respectively. (D) Schematic diagram of an enterocyte (left) and its brush border F-actin structure (right, magenta), showing the microvilli and terminal web. (E–G′′) Subcellular localization of Myo31DF-mEGFP (green in E and E′′), Myo61F-mRFP (green in F and F′′), and Myo95E-RB-FLAG (green in G and G′′), which were overexpressed in the larval midgut enterocytes. The F-actin-enriched apical domain was stained by fluorescently labeled phalloidin (magenta in E′, E′′, F′, F′′, G′, and G′′). Insets in E–G′′ are high magnifications of the areas shown by white squares. In E′, vm indicates visceral muscle. E′′, F′′, and G′′ are merged images of E and E′, F and F′, and G and G′, respectively. Bars, 10 μm.

Although the three class I myosin proteins were detected in both regions of the brush border, Myo31DF-mEGFP was enriched in the terminal web domain, and Myo61F-mRFP was enriched in the microvilli (Figure 5, D, E–E′′, and F–F′′), consistent with previous findings in which endogenous Myo31DF and Myo61F proteins were detected using specific antibodies (Morgan *et al.* 1995). We found that the distribution of Myo95E-RB-FLAG was punctate, distinct from that of Myo31DF-mEGFP and Myo61F-mRFP, although the puncta were detected primarily in both the microvilli and the terminal web domain (Figure 5, G–G′′). Therefore, although the head region of Myo95E has an atypical insertion, our results suggest that Myo95E, like Myo31DF and Myo61F, colocalizes with F-actin in a similar yet distinct subcellular location.

Myo31DF, Myo61DF, and Myo95E show overlapping but distinct subcellular distributions in the apical brush border of larval midgut enterocytes

It was previously reported that the endogenous Myo31DF and Myo61F are distinctly localized in the cells of the genital disc and that both the RNA knockdown and overexpression of *Myo61F* lead to a decreased Myo31DF protein signal detected by immunostaining (Petzoldt *et al.* 2012). In addition, our analysis above showed that the three class I myosin proteins colocalized with F-actin, but exhibited distinct subcellular distributions in the apical brush border of the larval midgut enterocytes (Figure 5, E–G′′). To further analyze the subcellular localization of these proteins, we next coexpressed the tagged myosin I proteins (*Myo31DF-mEGFP*, *Myo61F-mRFP*, and *Myo95E-RB-FLAG)* two at time and observed their localization.

In S2 cells, the coexpression of any two of the tagged myosins resulted in their colocalization in cytoplasmic aggregates (Figure 6, A–C). These observations were consistent with the above findings that all three class I myosin proteins similarly colocalized with F-actin in S2 cells (Figure 5, A and B). We then coexpressed these genes (two at a time) in the larval midgut enterocytes, where endogenous Myo31DF and Myo61F are enriched in the terminal web domain and the microvilli, respectively (Morgan *et al.* 1995). Here we found that Myo31DF-mEGFP was localized

to the terminal web domain and the microvilli, whereas Myo61F-mRFP was enriched in the microvilli but mostly excluded from the basal region (Figure 6, D–D′′′) corresponding to the terminal web domain (Figure 5D); these findings are largely consistent with a previous report (Morgan *et al.* 1995). In addition, as shown in the inset of Figure 6D′′, Myo31DF-mEGFP (in green), but not Myo61F-mRFP (in magenta), was detected along the terminal web domain (white arrowheads). When *Myo95E-RB-FLAG* was coexpressed with either *Myo31DF-mEGFP* or *Myo61F-mRFP*, the Myo95E-RB-FLAG was distributed more basally than the Myo31DF-mEGFP or Myo61F-mRFP (Figure 6, E–E′′′ and F–F′′′ and arrowheads in Figure 6, E′′ and F′′). We also found that the overexpression of these three myosin I genes did not affect the overall distribution of F-actin in the enterocytes, detected by phalloidin staining (Figure 6, D′′′–F′′′).

Discussion

Roles of class I myosins in Drosophila

In various organisms, the class I myosins often have overlapping functions, but can have distinct roles in certain cases (Osherov and May 2000; Kim and Flavell 2008). In simple organisms, such as yeast and *Dictyostelium*, the class I myosins have overlapping functions in various cellular processes, in which the actin cytoskeleton plays crucial roles (Osherov and May 2000; Kim and Flavell 2008). Knock-out or knock-in mice for several class I myosin genes (myosins IA, IC, IE, and IF) have been generated (Stauffer *et al.* 2005; Tyska *et al.* 2005; Kim *et al.* 2006; Krendel *et al.* 2009; Venit *et al.* 2013) and studies of these mice indicated that these genes are dispensable for survival under normal conditions, when disrupted separately (Tyska *et al.* 2005; Kim *et al.* 2006; Krendel *et al.* 2009). However, the results of deleting all class I myosin genes have not been reported in any metazoan.

D. melanogaster has three class I myosin genes, *Myo31DF*, *Myo61F*, and *Myo95E* (Tzolovsky *et al.* 2002). Taking advantage of the fact that *Drosophila* has a relatively small number of class I myosin genes, we obtained or generated mutants of each myosin gene, which were defined as null mutations based on their molecular lesions. We then generated various combinations of the mutants and analyzed their phenotypes.

We found that flies containing mutations in all three type I myosin genes were viable and fertile. *Schizosaccharomyces pombe* has a single class I myosin gene, and a loss-of-function mutation in this gene is not lethal under normal conditions (Lee *et al.* 2000; Toya *et al.* 2001). *S. cerevisiae* has two class I myosin genes, and cells lacking both of these genes are also viable (Geli and Riezman 1996; Goodson *et al.* 1996). Similarly, our results demonstrated that class I myosin genes are not essential for survival in *Drosophila*. However, we found that the hatching and survival rates were decreased in these mutants and their double and triple mutants. The decreased survival rate might be explained by the previous finding that a *Drosophila* *Myo61F* homozygous mutant exhibits midgut brush border defects, which are unlikely to be attributed to *Myo61F*'s role in LR asymmetric development (Hegan *et al.* 2007). This brush border defect causes an increased susceptibility to lethal infection caused by bacterial pathogens (Hegan *et al.* 2007). However, due to the broad variability of this defect in the structure of the brush border, we could not analyze whether this phenotype was enhanced in the double and triple mutants (data not shown). We also observed a 50% reduction in the hatching rate of the triple-mutant embryos, which may not be explained by the defect of the brush border. However, we did not find specific defects in their embryonic development, other than the LR inversion of the embryonic gut (shown above).

Redundant roles of Myo31DF and Myo61F in LR asymmetric development of the male genitalia

In the *Myo31DF* homozygous mutant, the LR asymmetry of various, but not all, organs assumes the mirror image of the wild type (Hozumi *et al.* 2006; Speder *et al.* 2006). Thus, it was previously proposed that the sinistral state of LR asymmetry may be a default state in organ development that is reversed by the wild-type function of *Myo31DF* (Hozumi *et al.* 2006; Speder *et al.* 2006). The overexpression of *Myo61F* also induces sinistral LR asymmetry in various organs, including the embryonic gut and male genitalia (Hozumi *et al.* 2006; Speder *et al.* 2006; Petzoldt *et al.* 2012). This activity was thought to involve the inhibition of Myo31DF's dextral activity (Hozumi *et al.* 2006; Speder *et al.* 2006; Petzoldt *et al.* 2012). Myo31DF physically interacts with β-catenin, and this interaction is required for the LR activity of Myo31DF (Petzoldt *et al.* 2012). In the male genitalia, overexpressed Myo61F antagonizes Myo31DF's activity by preventing Myo31DF's interaction with β-catenin (Petzoldt *et al.* 2012). However, in this study, we found that *Myo61F* overexpression in the *Myo31DF* null mutant embryos, 80% of which showed sinistral phenotypes, increased this percentage to 100% (Figure 3F). This finding suggested that *Myo61F* exerts its sinistral activity even in the absence of *Myo31DF*. The target of *Myo61F* overexpression responsible for this activity is currently unknown.

Although *Myo61F* overexpression reverses the dextral LR asymmetry in the embryonic gut and male genitalia (Hozumi *et al.* 2006; Petzoldt *et al.* 2012), our loss-of-function analysis revealed that Myo61F shared an overlapping dextral activity with Myo31DF in the LR asymmetric development of the male genitalia. The *Myo31DF/Myo61F* double mutant showed a significant increase ($P < 0.01$) in the sinistral rotation phenotype compared with that of the single *Myo31DF* mutant, although the *Myo61F* mutant alone did not show LR defects. A similar increase in sinistral activity was observed in the *Myo31DF/Myo61F/Myo95E* triple mutant, with the same statistical significance ($P < 0.01$). The *Myo61F* activity deduced from our loss-of-function analysis (dextral activity) was inconsistent with the activity associated with its overexpression (sinistral activity). Thus, even though

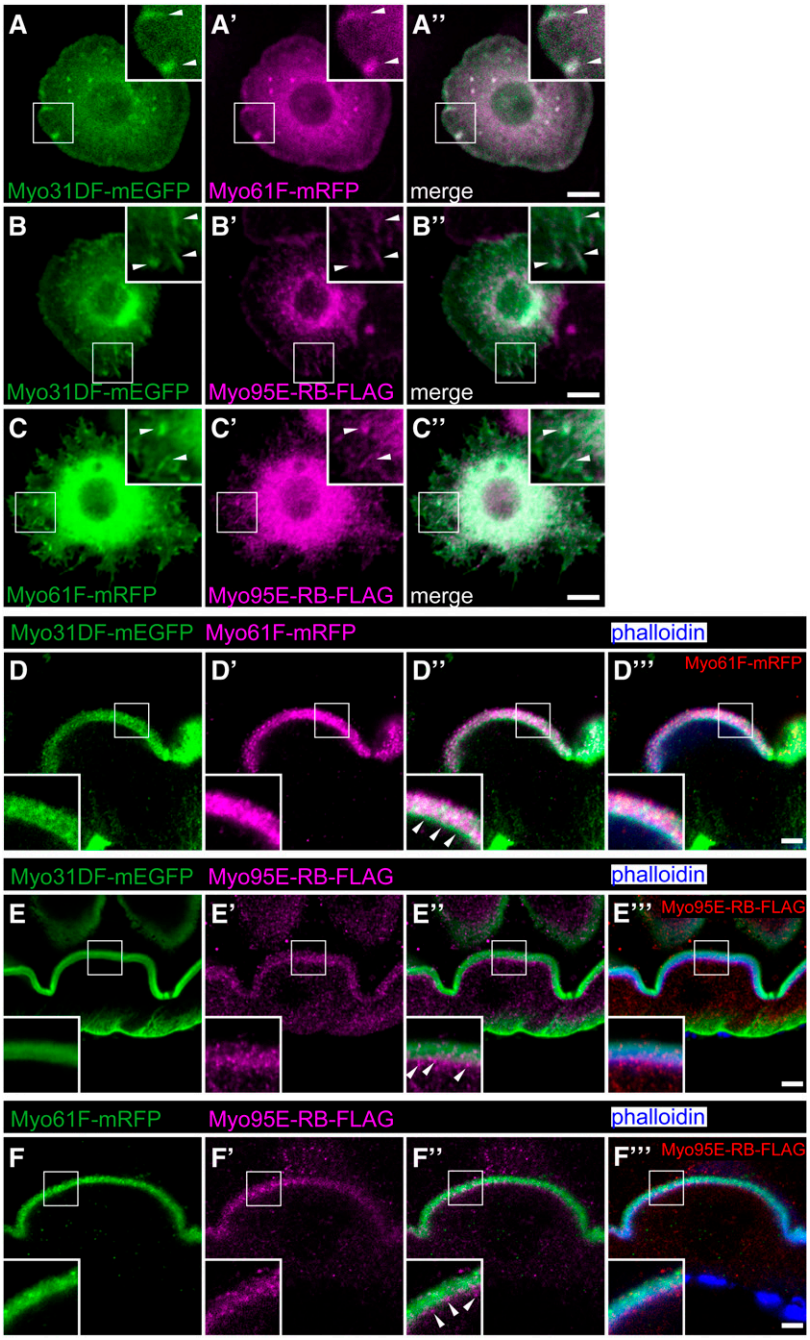

Figure 6 Colocalization of *Drosophila* class I myosin proteins. (A–C′′) S2 cells coexpressing *Myo31DF-mEGFP* (green) and *Myo61F-mRFP* (magenta) (A–A′′), *Myo31DF-mEGFP* (green) and *Myo95E-RB-FLAG* (magenta) (B–B′′), and *Myo61F-mRFP* (green) and *Myo95E-RB-FLAG* (magenta) (C–C′′). Insets in A–C′′ are high magnifications of the areas shown by white squares, and arrowheads in the insets indicate colocalization of the two coexpressed class I myosin proteins. A′′, B′′, and C′′ are merged images of A and A′, B and B′, and C and C′, respectively. (D–F′′′) The larval anterior midgut epithelial cells coexpressing *Myo31DF-mEGFP* (green) and *Myo61F-mRFP* (magenta) (D–D′′′), *Myo31DF-mEGFP* (green) and *Myo95E-RB-FLAG* (magenta) (E–E′′′), and *Myo61F-mRFP* (green) and *Myo95E-RB-FLAG* (magenta) (F–F′′′) were stained with fluorescently labeled phalloidin (blue). Insets in D–F′′′ are high magnifications of the areas shown by white squares. D′′, E′′, and F′′ are merged images of D and D′, E and E′, and F and F′, respectively. D′′′, E′′′, and F′′′ are merged images of fluorescently labeled phalloidin (blue) and D′′, E′′, and F′′, respectively. Bars, 5 μm.

Myo61F overexpression induces LR inversion, it is likely that *Myo61F* has dextral activity in the LR asymmetric development of the male genitalia under physiological conditions. Notably, the *Myo61F* mutation did not affect LR asymmetric development of the embryonic gut, even in combination with *Myo31DF* and *Myo95E* mutations, suggesting that the role of *Myo61F* in LR asymmetric development is tissue specific. This tissue-specific function may be due to the tissue specificity of *Myo61F* gene expression, given that *Myo61F* was not detected in the hg by *in situ* hybridization at stage 12, when the expression of *Myo31DF* is required for the normal LR asymmetric development of this organ (Hozumi *et al.* 2008).

Drosophila Myo95E is a Myosin IB isoform

The Myo95E protein has a large insertion in the head region. Except for this insertion, Myo95E is most similar to Myosin IB (MyoIB), which is conserved from *Drosophila* to mammals (Tzolovsky *et al.* 2002). This insertion is found in the MyoIB of Diptera, including flies and mosquitoes [*Ceratitis capitata*, NCBI reference sequence XP_004533658; *Aedes aegypti*, XP_001663112.1 (Nene *et al.* 2007)], but not in the MyoIB of beetles and lice (Tribolium Genome Sequencing Consortium *et al.* 2008; Kirkness *et al.* 2010; Keeling *et al.* 2013). No obvious MyoIB ortholog is found in bees, ants, butterflies, or moths, whose genomes have been completely

sequenced (Honeybee Genome Sequencing Consortium 2006; Xia *et al.* 2008; Bonasio *et al.* 2010; Werren *et al.* 2010; Nygaard *et al.* 2011; Zhan *et al.* 2011). Thus, we speculated that the insertion was acquired by MyoIB relatively recently during insect evolution.

A role for *Myo95E* was not observed in the present study. However, the expression of *Myo95E* was detected in the embryonic nervous system, in contrast to *Myo31DF* and *Myo61F*, which were barely detected there. Therefore, we cannot exclude the possibility that *Myo95E* plays a role in the physiology of neural cells, which may not have been detected by our analysis.

Acknowledgments

We are grateful to S. Noselli for providing the *Myo31DF*^{K2} and *UAS-Myo31DF-GFP* lines. We also thank the *Drosophila* Genetic Resource Center at the Kyoto Institute of Technology, the Bloomington *Drosophila* Stock Center at Indiana University, and the Development Studies Hybridoma Bank at the University of Iowa for providing flies and antibodies. We thank members of the Matsuno laboratory for critical comments and discussions. This work was supported by The Ministry of Education, Culture, Sports, Science and Technology (MEXT) Grants-in-Aid for Scientific Research (KAKENHI) grant 22127004 and the National Institute of Genetics (NIG) Cooperative Research Program (2007-A51 and 2009-A79).

Literature Cited

Adams, M. D., S. E. Celniker, R. A. Holt, C. A. Evans, J. D. Gocayne *et al.*, 2000 The genome sequence of *Drosophila melanogaster*. Science 287: 2185–2195.

Almeida, C. G., A. Yamada, D. Tenza, D. Louvard, G. Raposo *et al.*, 2011 Myosin 1b promotes the formation of post-Golgi carriers by regulating actin assembly and membrane remodelling at the *trans*-Golgi network. Nat. Cell Biol. 13: 779–789.

Ashburner, M., K. G. Golic, and R. S. Hawley, 1989 *Drosophila: A Laboratory Handbook*, Ed. 2. Cold Spring Harbor Laboratory Press, Cold Spring Harbor, NY.

Barylko, B., D. D. Binns, and J. P. Albanesi, 2000 Regulation of the enzymatic and motor activities of myosin I. Biochim. Biophys. Acta 1496: 23–35.

Berg, J. S., B. C. Powell, and R. E. Cheney, 2001 A millennial myosin census. Mol. Biol. Cell 12: 780–794.

Bischof, J., R. K. Maeda, M. Hediger, F. Karch, and K. Basler, 2007 An optimized transgenesis system for Drosophila using germ-line-specific phiC31 integrases. Proc. Natl. Acad. Sci. USA 104: 3312–3317.

Bonasio, R., G. Zhang, C. Ye, N. S. Mutti, X. Fang *et al.*, 2010 Genomic comparison of the ants *Camponotus floridanus* and *Harpegnathos saltator*. Science 329: 1068–1071.

Bose, A., A. Guilherme, S. I. Robida, S. M. Nicoloro, Q. L. Zhou *et al.*, 2002 Glucose transporter recycling in response to insulin is facilitated by myosin Myo1c. Nature 420: 821–824.

Brand, A. H., and N. Perrimon, 1993 Targeted gene expression as a means of altering cell fates and generating dominant phenotypes. Development 118: 401–415.

Campbell, R. E., O. Tour, A. E. Palmer, P. A. Steinbach, G. S. Baird *et al.*, 2002 A monomeric red fluorescent protein. Proc. Natl. Acad. Sci. USA 99: 7877–7882.

Chen, A. H., D. A. Stephan, T. Hasson, K. Fukushima, C. M. Nelissen *et al.*, 2001 MYO1F as a candidate gene for nonsyndromic deafness, DFNB15. Arch. Otolaryngol. Head Neck Surg. 127: 921–925.

Chen, C. L., Y. Wang, H. Sesaki, and M. Iijima, 2012 Myosin I links PIP3 signaling to remodeling of the actin cytoskeleton in chemotaxis. Sci. Signal. 5: ra10.

Cherbas, L., and P. Cherbas, 2000 *Drosophila* cell culture and transformation, pp. 373–387 in *Drosophila Protocols*, edited by W. Sullivan, M. Ashburner, and R. S. Hawley. Cold Spring Harbor Laboratory Press, Cold Spring Harbor, NY.

Coluccio, L. M., 1997 Myosin I. Am. J. Physiol. 273: C347–C359.

Coutelis, J. B., C. Géminard, P. Spéder, M. Suzanne, A. G. Petzoldt *et al.*, 2013 *Drosophila* left/right asymmetry establishment is controlled by the Hox gene *Abdominal-B*. Dev. Cell 24: 89–97.

Donaudy, F., A. Ferrara, L. Esposito, R. Hertzano, O. Ben-David *et al.*, 2003 Multiple mutations of MYO1A, a cochlear-expressed gene, in sensorineural hearing loss. Am. J. Hum. Genet. 72: 1571–1577.

Fan, Y., S. M. Eswarappa, M. Hitomi, and P. L. Fox, 2012 Myo1c facilitates G-actin transport to the leading edge of migrating endothelial cells. J. Cell Biol. 198: 47–55.

Fath, K. R., S. N. Mamajiwalla, and D. R. Burgess, 1993 The cytoskeleton in development of epithelial cell polarity. J. Cell Sci. Suppl. 17: 65–73.

Foronda, D., B. Estrada, L. de Navas, and E. Sánchez-Herrero, 2006 Requirement of *Abdominal-A* and *Abdominal-B* in the developing genitalia of *Drosophila* breaks the posterior downregulation rule. Development 133: 117–127.

Fyrberg, C., J. Becker, P. Barthmaier, J. Mahaffey, and E. Fyrberg, 1997 A *Drosophila* muscle-specific gene related to the mouse quaking locus. Gene 197: 315–323.

Geli, M. I., and H. Riezman, 1996 Role of type I myosins in receptor-mediated endocytosis in yeast. Science 272: 533–535.

Gillespie, P. G., 2004 Myosin I and adaptation of mechanical transduction by the inner ear. Philos. Trans. R. Soc. Lond. B Biol. Sci. 359: 1945–1951.

Gillespie, P. G., and J. L. Cyr, 2004 Myosin-1c, the hair cell's adaptation motor. Annu. Rev. Physiol. 66: 521–545.

Goodson, H. V., B. L. Anderson, H. M. Warrick, L. A. Pon, and J. A. Spudich, 1996 Synthetic lethality screen identifies a novel yeast myosin gene (*MYO5*): myosin I proteins are required for polarization of the actin cytoskeleton. J. Cell Biol. 133: 1277–1291.

Grigliatti, T. A., 1998 Transposons—gene tagging and mutagenesis, pp. 85–107 in *Drosophila: A Practical Approach*, Ed. 2, edited by D. B. Roberts. IRL Press, Oxford.

Hayashi, T., and R. Murakami, 2001 Left-right asymmetry in *Drosophila melanogaster* gut development. Dev. Growth Differ. 43: 239–246.

Hegan, P. S., V. Mermall, L. G. Tilney, and M. S. Mooseker, 2007 Roles for *Drosophila melanogaster* myosin IB in maintenance of enterocyte brush-border structure and resistance to the bacterial pathogen *Pseudomonas entomophila*. Mol. Biol. Cell 18: 4625–4636.

Honeybee Genome Sequencing Consortium, 2006 Insights into social insects from the genome of the honeybee *Apis mellifera*. Nature 443: 931–949.

Hopp, T. P., K. S. Prickett, V. L. Price, R. T. Libby, C. J. March *et al.*, 1988 A short polypeptide marker sequence useful for recombinant protein identification and purification. Nat. Biotechnol. 6: 1204–1210.

Hozumi, S., R. Maeda, K. Taniguchi, M. Kanai, S. Shirakabe *et al.*, 2006 An unconventional myosin in *Drosophila* reverses the default handedness in visceral organs. Nature 440: 798–802.

Hozumi, S., R. Maeda, M. Taniguchi-Kanai, T. Okumura, K. Taniguchi *et al.*, 2008 Head region of unconventional myosin I family members is responsible for the organ-specificity of their roles in left-right polarity in *Drosophila*. Dev. Dyn. 237: 3528–3537.

Iwaki, D. D., and J. A. Lengyel, 2002 A Delta-Notch signaling border regulated by Engrailed/Invected repression specifies boundary cells in the *Drosophila* hindgut. Mech. Dev. 114: 71–84.

Johnson, R. L., J. K. Grenier, and M. P. Scott, 1995 *patched* overexpression alters wing disc size and pattern: transcriptional and post-transcriptional effects on *hedgehog* targets. Development 121: 4161–4170.

Jung, G., X. Wu, and J. A. Hammer, 3rd, 1996 Dictyostelium mutants lacking multiple classic myosin I isoforms reveal combinations of shared and distinct functions. J. Cell Biol. 133: 305–323.

Keeling, C. I., M. M. Yuen, N. Y. Liao, T. Roderick Docking, S. K. Chan *et al.*, 2013 Draft genome of the mountain pine beetle, *Dendroctonus ponderosae Hopkins*, a major forest pest. Genome Biol. 14: R27.

Kim, S. V., and R. A. Flavell, 2008 Myosin I: from yeast to human. Cell. Mol. Life Sci. 65: 2128–2137.

Kim, S. V., W. Z. Mehal, X. Dong, V. Heinrich, M. Pypaert *et al.*, 2006 Modulation of cell adhesion and motility in the immune system by Myo1f. Science 314: 136–139.

Kirkness, E. F., B. J. Haas, W. Sun, H. R. Braig, M. A. Perotti *et al.*, 2010 Genome sequences of the human body louse and its primary endosymbiont provide insights into the permanent parasitic lifestyle. Proc. Natl. Acad. Sci. USA 107: 12168–12173.

Krendel, M., and M. S. Mooseker, 2005 Myosins: tails (and heads) of functional diversity. Physiology 20: 239–251.

Krendel, M., S. V. Kim, T. Willinger, T. Wang, M. Kashgarian *et al.*, 2009 Disruption of Myosin 1e promotes podocyte injury. J. Am. Soc. Nephrol. 20: 86–94.

Kuranaga, E., T. Matsunuma, H. Kanuka, K. Takemoto, A. Koto *et al.*, 2011 Apoptosis controls the speed of looping morphogenesis in *Drosophila* male terminalia. Development 138: 1493–1499.

Lee, W. L., M. Bezanilla, and T. D. Pollard, 2000 Fission yeast myosin-I, Myo1p, stimulates actin assembly by Arp2/3 complex and shares functions with WASp. J. Cell Biol. 151: 789–800.

Ligoxygakis, P., M. Strigini, and M. Averof, 2001 Specification of left-right asymmetry in the embryonic gut of *Drosophila*. Development 128: 1171–1174.

McConnell, R. E., and M. J. Tyska, 2010 Leveraging the membrane - cytoskeleton interface with myosin-1. Trends Cell Biol. 20: 418–426.

McConnell, R. E., J. N. Higginbotham, D. A. Shifrin, Jr., D. L. Tabb, R. J. Coffey *et al.*, 2009 The enterocyte microvillus is a vesicle-generating organelle. J. Cell Biol. 185: 1285–1298.

Mermall, V., P. L. Post, and M. S. Mooseker, 1998 Unconventional myosins in cell movement, membrane traffic, and signal transduction. Science 279: 527–533.

Miyashita, T., Y. Oda, J. Horiuchi, J. C. Yin, T. Morimoto *et al.*, 2012 Mg(2+) block of Drosophila NMDA receptors is required for long-term memory formation and CREB-dependent gene expression. Neuron 74: 887–898.

Molloy, J. E., J. E. Burns, J. Kendrick-Jones, R. T. Tregear, and D. C. White, 1995 Movement and force produced by a single myosin head. Nature 378: 209–212.

Morgan, N. S., D. M. Skovronsky, S. Artavanis-Tsakonas, and M. S. Mooseker, 1994 The molecular cloning and characterization of *Drosophila melanogaster* myosin-IA and myosin-IB. J. Mol. Biol. 239: 347–356.

Morgan, N. S., M. B. Heintzelman, and M. S. Mooseker, 1995 Characterization of myosin-IA and myosin-IB, two unconventional myosins associated with the *Drosophila* brush border cytoskeleton. Dev. Biol. 172: 51–71.

Nambiar, R., R. E. McConnell, and M. J. Tyska, 2009 Control of cell membrane tension by myosin-I. Proc. Natl. Acad. Sci. USA 106: 11972–11977.

Nene, V., J. R. Wortman, D. Lawson, B. Haas, C. Kodira *et al.*, 2007 Genome sequence of *Aedes aegypti*, a major arbovirus vector. Science 316: 1718–1723.

Novak, K. D., M. D. Peterson, M. C. Reedy, and M. A. Titus, 1995 *Dictyostelium* myosin I double mutants exhibit conditional defects in pinocytosis. J. Cell Biol. 131: 1205–1221.

Nygaard, S., G. Zhang, M. Schiøtt, C. Li, Y. Wurm *et al.*, 2011 The genome of the leaf-cutting ant *Acromyrmex echinatior* suggests key adaptations to advanced social life and fungus farming. Genome Res. 21: 1339–1348.

O'Kane, C. J., 1998 Enhancer traps, pp. 131–178 in *Drosophila: A Practical Approach*, Ed. 2, edited by D. B. Roberts. IRL Press, Oxford.

Osherov, N., and G. S. May, 2000 In vivo function of class I myosins. Cell Motil. Cytoskeleton 47: 163–173.

Parks, A. L., K. R. Cook, M. Belvin, N. A. Dompe, R. Fawcett *et al.*, 2004 Systematic generation of high-resolution deletion coverage of the *Drosophila melanogaster* genome. Nat. Genet. 36: 288–292.

Pestic-Dragovich, L., L. Stojiljkovic, A. A. Philimonenko, G. Nowak, Y. Ke *et al.*, 2000 A myosin I isoform in the nucleus. Science 290: 337–341.

Petzoldt, A. G., J. B. Coutelis, C. Géminard, P. Spéder, M. Suzanne *et al.*, 2012 DE-Cadherin regulates unconventional Myosin ID and Myosin IC in *Drosophila* left-right asymmetry establishment. Development 139: 1874–1884.

Philimonenko, V. V., J. Zhao, S. Iben, H. Dingová, K. Kyselá *et al.*, 2004 Nuclear actin and myosin I are required for RNA polymerase I transcription. Nat. Cell Biol. 6: 1165–1172.

Phillips, M. D., and G. H. Thomas, 2006 Brush border spectrin is required for early endosome recycling in *Drosophila*. J. Cell Sci. 119: 1361–1370.

Rubin, G. M., L. Hong, P. Brokstein, M. Evans-Holm, E. Frise *et al.*, 2000 A *Drosophila* complementary DNA resource. Science 287: 2222–2224.

Sellers, J. R., 2000 Myosins: a diverse superfamily. Biochim. Biophys. Acta 1496: 3–22.

Shyamala, B. V., and K. M. Bhat, 2002 A positive role for Patched-Smoothened signaling in promoting cell proliferation during normal head development in *Drosophila*. Development 129: 1839–1847.

Sokac, A. M., C. Schietroma, C. B. Gundersen, and W. M. Bement, 2006 Myosin-1c couples assembling actin to membranes to drive compensatory endocytosis. Dev. Cell 11: 629–640.

Speder, P., G. Adam, and S. Noselli, 2006 Type ID unconventional myosin controls left-right asymmetry in *Drosophila*. Nature 440: 803–807.

Spradling, A. C., 1986 P element-mediated transformation, pp. 175–197 in *Drosophila: A Practical Approach*, edited by D. B. Roberts. IRL Press, Oxford.

Stapleton, M., G. Liao, P. Brokstein, L. Hong, P. Carninci *et al.*, 2002 The *Drosophila* gene collection: identification of putative full-length cDNAs for 70% of *D. melanogaster* genes. Genome Res. 12: 1294–1300.

Stauffer, E. A., J. D. Scarborough, M. Hirono, E. D. Miller, K. Shah *et al.*, 2005 Fast adaptation in vestibular hair cells requires myosin-1c activity. Neuron 47: 541–553.

Strutt, H., C. Thomas, Y. Nakano, D. Stark, B. Neave *et al.*, 2001 Mutations in the sterol-sensing domain of Patched suggest a role for vesicular trafficking in Smoothened regulation. Curr. Biol. 11: 608–613.

Suzanne, M., A. G. Petzoldt, P. Speder, J. B. Coutelis, and H. Steller *et al.*, 2010 Coupling of apoptosis and L/R patterning controls stepwise organ looping. Curr. Biol. 20: 1773–1778.

Taniguchi, K., S. Hozumi, R. Maeda, T. Okumura, and K. Matsuno, 2007 Roles of type I myosins in *Drosophila* handedness. Fly 1: 287–290.

Taniguchi, K., R. Maeda, T. Ando, T. Okumura, N. Nakazawa *et al.*, 2011 Chirality in planar cell shape contributes to left-right asymmetric epithelial morphogenesis. Science 333: 339–341.

Toya, M., F. Motegi, K. Nakano, I. Mabuchi, and M. Yamamoto, 2001 Identification and functional analysis of the gene for type I myosin in fission yeast. Genes Cells 6: 187–199.

Tribolium Genome Sequencing Consortium, S. Richards, R. A. Gibbs, G. M. Weinstock, S. J. Brown *et al.*, 2008 The genome of the model beetle and pest *Tribolium castaneum*. Nature 452: 949–955.

Tyska, M. J., A. T. Mackey, J. D. Huang, N. G. Copeland, N. A. Jenkins *et al.*, 2005 Myosin-1a is critical for normal brush border structure and composition. Mol. Biol. Cell 16: 2443–2457.

Tzolovsky, G., H. Millo, S. Pathirana, T. Wood, and M. Bownes, 2002 Identification and phylogenetic analysis of *Drosophila melanogaster* myosins. Mol. Biol. Evol. 19: 1041–1052.

Venit, T., R. Dzijak, A. Kalendová, M. Kahle, J. RohoŽková *et al.*, 2013 Mouse nuclear myosin I knock-out shows interchangeability and redundancy of myosin isoforms in the cell nucleus. PLoS ONE 8: e61406.

Werren, J. H., S. Richards, C. A. Desjardins, O. Niehuis, J. Gadau *et al.*, 2010 Functional and evolutionary insights from the genomes of three parasitoid *Nasonia* species. Science 327: 343–348.

Xia, Q., J. Wang, Z. Zhou, R. Li, W. Fan *et al.*, 2008 The genome of a lepidopteran model insect, the silkworm *Bombyx mori*. Insect Biochem. Mol. Biol. 38: 1036–1045.

Zadro, C., M. S. Alemanno, E. Bellacchio, R. Ficarella, F. Donaudy *et al.*, 2009 Are MYO1C and MYO1F associated with hearing loss? Biochim. Biophys. Acta 1792: 27–32.

Zhan, S., C. Merlin, J. L. Boore, and S. M. Reppert, 2011 The monarch butterfly genome yields insights into long-distance migration. Cell 147: 1171–1185.

Communicating editor: W. T. Sullivan

GENETICS

Supporting Information
http://www.genetics.org/lookup/suppl/doi:10.1534/genetics.115.174698/-/DC1

Class I Myosins Have Overlapping and Specialized Functions in Left-Right Asymmetric Development in *Drosophila*

Takashi Okumura, Takeshi Sasamura, Momoko Inatomi, Shunya Hozumi, Mitsutoshi Nakamura, Ryo Hatori, Kiichiro Taniguchi, Naotaka Nakazawa, Emiko Suzuki, Reo Maeda, Tomoko Yamakawa, and Kenji Matsuno

DOI: 10.1534/genetics.115.174698

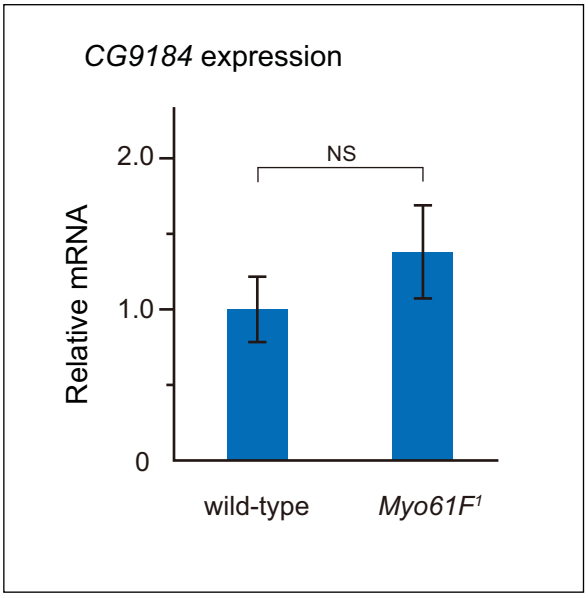

Figure S1 Expression of *CG9184* in wild-type or *Myo61F*^{1} homozygous pupae 23-25 h after pupation, quantified by real-time PCR. The amount of *CG9184* transcript was normalized to that of *Gapdh1*. The amount of *CG9184* transcript relative to that of wild-type (adjusted to 1.0) is shown. Average values of triplicate determinations are shown. NS: not significant by t-test.

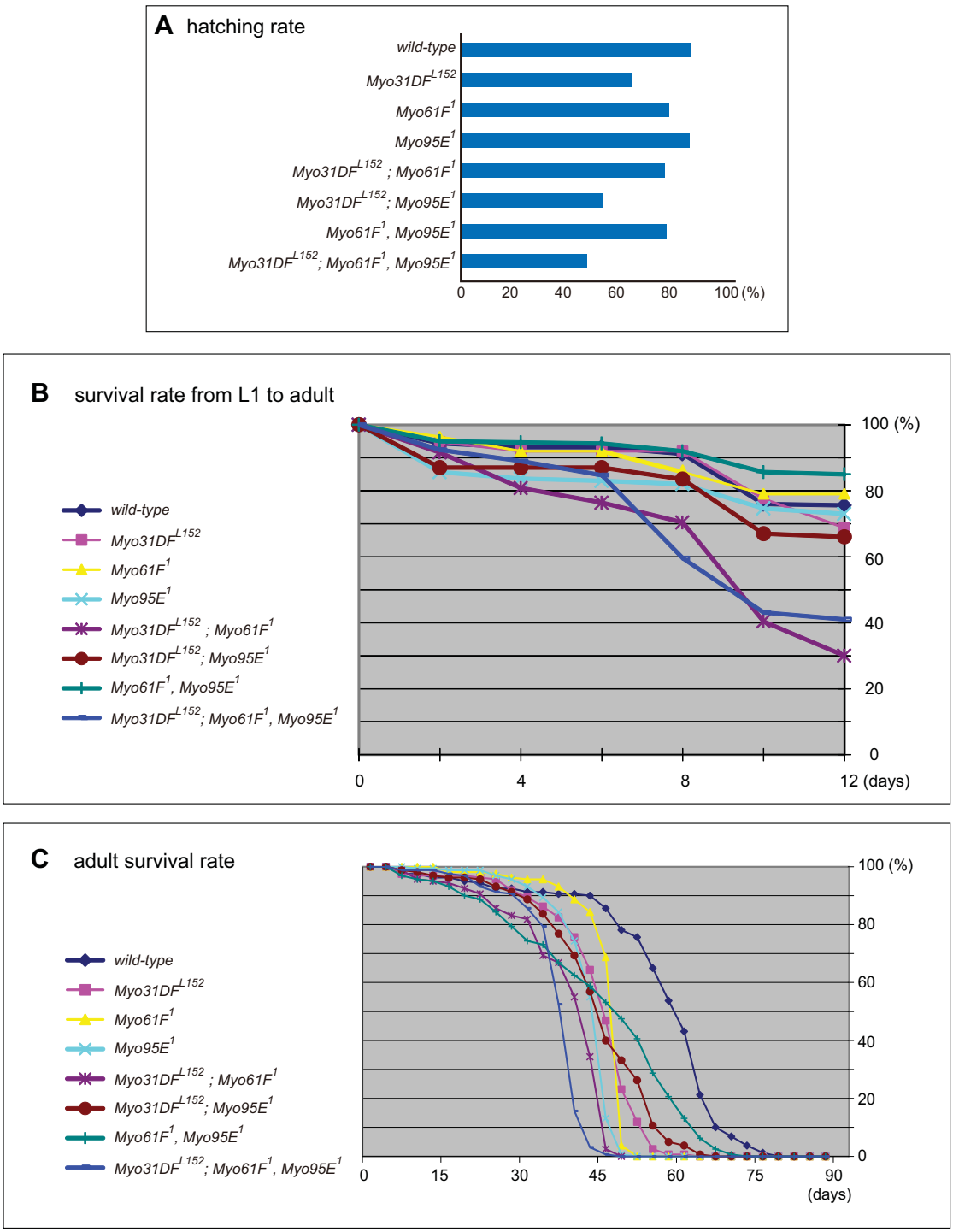

Figure S2 Hatching and survival rates of class I myosin mutants. (A) Bar graph depicting hatching rates. (B and C) Line graphs depicting first-instar larva to adult survival rates (B) and adult survival rates (C). Genotypes are indicated at left.

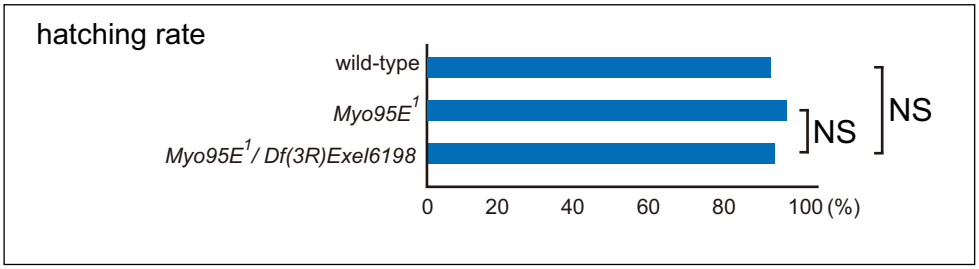

Figure S3 Hatching rate of wild-type, *Myo95E*^{1} homozygous, and *Myo95E*^{1}*/Df(3R)Exel6198* trans-heterozygous flies. Bar graph depicts the hatching rate. *Df(3R)Exel6198* is a deletion mutant uncovering the *Myo95E* locus. Genotypes are indicated at left. NS: not significant by t-test.

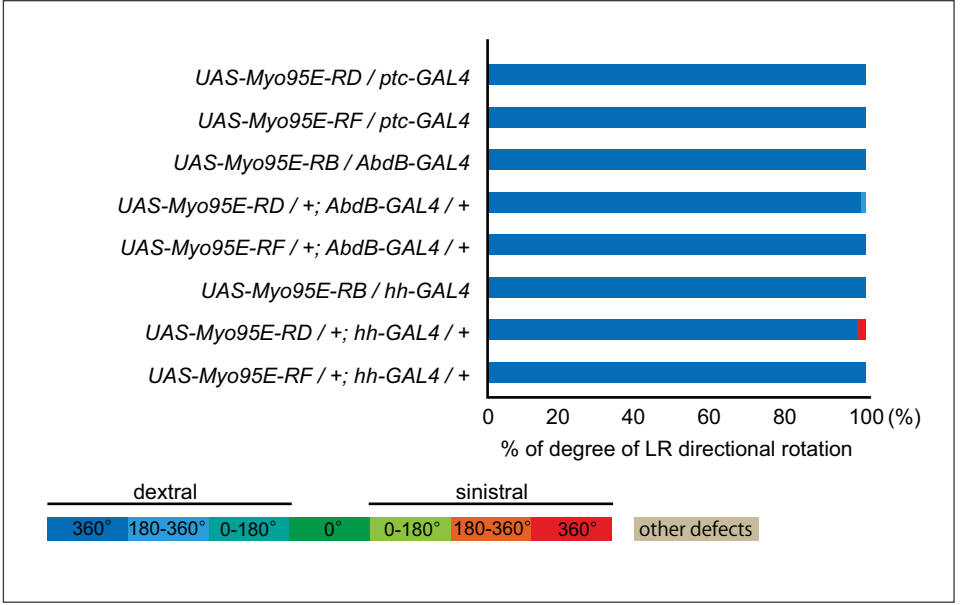

Figure S4 LR phenotypes of male genitalia under the overexpression of *Myo95E* isoforms. The overexpression of *Myo95E-RB*, *-RD*, and *-RF* driven by *ptc-GAL4*, *Abd-B-GAL4*, and *hh-GAL4* are shown. Bar graphs show the frequency (%) of dextral and sinistral rotation phenotypes observed in the male genital plate, color coded according to the categories shown at the bottom. Genotypes are indicated at left.